# Joint MIMO Communications and Sensing with Hybrid Beamforming Architecture and OFDM Waveform Optimization

Sahan Damith Liyanaarachchi, *Graduate Student Member, IEEE,* Taneli Riihonen, *Senior Member, IEEE,* Carlos Baquero Barneto, *Graduate Student Member, IEEE,* and Mikko Valkama, *Fellow, IEEE*

***Abstract*—In this article, we consider a multiple-input multiple-output (MIMO) transceiver performing joint communications and sensing (JCAS) using fifth-generation New Radio (5G NR) standard-compliant orthogonal frequency-division multiplexing (OFDM) waveforms. Communication links are maintained with users having multiple spatial data streams over frequency-selective non-line-of-sight channels while simultaneously transmitting separate spatial data streams to different sensing directions, where a portion of the communication data streams' power is reallocated to the sensing data streams. The received reflections from the environment due to all transmit (TX) streams are used to obtain range–velocity and range–angle maps. Through optimizing the TX precoding and receive combining, inter-user, intra-user, and radar–communications interference are also canceled. In addition, streams transmitted in the sensing directions are optimized to minimize the lower bounds of direction-of-arrival and delay estimates jointly, and the solution is analytically derived. The simulation results illustrate that the JCAS system can reliably perform target detection while minimizing lower bounds compared with a communications-only scenario. Further, the detection probability and estimation errors of sensing can be improved while also controlling the communications capacity of the OFDM waveform, thereby indicating the need to appropriately choose the optimization parameters to obtain an optimal trade-off.**

***Index Terms*—5G NR, JCAS, joint communications and sensing, MIMO, OFDM, radar.**

## I. Introduction

JOINT communications and sensing (JCAS) will be crucial in future sixth-generation (6G) systems [1]. Some good examples of leveraging modern communications systems for sensing are in [2]–[4]. To facilitate joint operation, the available resources, e.g., frequency spectrum, transmit (TX) power, and TX time duration, are generally shared mutually between the two sub-systems [5]. Hence, the inherent trade-off between communications and sensing depends mainly on the resources allocated to either sub-system [6]–[8]. It is thus vital to utilize those resources optimally rather than in a sub-optimal manner which degrades the performance of both sub-systems [9]. Some examples of the optimal trade-off are discussed in [4], [10] regarding sharing the bandwidth and in [11], [12] on sharing the TX beampattern. In addition, good surveys on JCAS can be found in [1], [5], [8], [13].

With the emergence of fifth-generation (5G) networks, communications systems started to operate at mm-wave frequencies due to the existence of more spectrum for their operations [14]. Generally in these mm-wave frequencies, multiple-input multiple-output (MIMO) antenna arrays are used, overcoming the high attenuation [15]. In addition, multiple users with multiple TX data streams can be catered using spatial multiplexing [16], providing high capacities to the users [17]. However, when multiple users with multiple data streams are involved, streams of one user interfere with themselves (i.e., intra-user interference), while also interfering with other users' streams (i.e., inter-user interference), and they need to be minimized to reap the full benefits of MIMO. Typically, interference cancellation is achieved by optimizing the TX precoding and/or receive (RX) combining [18] such that they/it also maximize/s sum capacity of the users for a fixed TX power or minimize/s the TX power for a fixed quality of service [19]. For instance, the work in [20] minimizes the inter-user interference by applying null-space projection to TX beamforming in a line-of-sight scenario. The authors in [18], [21] design both TX precoders and RX combiners such that sum spectral efficiency is maximized.

The MIMO counterpart for sensing is the MIMO radar, where different waveforms are transmitted from the TX antennas. There are generally two types, the statistical MIMO radar [22] and the coherent MIMO radar [23], and the latter is the focus of this article. In coherent MIMO radar, TX antennas are closely situated, and as a result, the radar channel between all transmitter–receiver pairs is essentially the same, with some phase difference. It is more suitable for scenarios where the target can be modeled as a point target. It also generally has a fully digital architecture, and sensing benefits from many advantages, such as unambiguous detection of multiple targets, i.e., parameter identifiability [24], increased resolution [25], [26], and better detection of targets with low velocity [24].

Much research is currently focused on JCAS with MIMO arrays [27]. Since orthogonal frequency-division multiplexing (OFDM) is the candidate waveform for modern communica-

Manuscript received August 05, 2022; revised January 17, 2023, and May 29, 2023; accepted June 18, 2023. Date of publication Month XX, 2023; date of current version June 26, 2023. The editor coordinating the review of this paper and approving it for publication was Batu Chalise. *(Corresponding author: Sahan Damith Liyanaarachchi.)*

S. D. Liyanaarachchi was with the Unit of Electrical Engineering, Tampere University, Finland. He is now with the Nokia Bell Labs, Espoo, Finland (e-mail: sahan.liyanaarachchi@nokia-bell-labs.com).

T. Riihonen, C. Baquero Barneto, and M. Valkama are with the Unit of Electrical Engineering, Tampere University, Finland.

This research was partially supported by the Research Council of Finland (grants #315858, #341489, and #346622) and the Doctoral School of Tampere University.

tions systems, e.g., 5G and potentially for 6G, these works focus on performing sensing using OFDM waveforms. Apart from the advantages OFDM provides for communications, e.g., efficient channel equalization and ease of multiplexing over time and frequency, it is also advantageous in sensing. Namely, OFDM radar processing in single-input single-output (SISO) systems involves applying the discrete Fourier transform (DFT) and its inverse to obtain the range and velocity estimates separately [7]. Hence, the OFDM radar processing is computationally efficient, while the accuracy of range estimation is not degraded upon the limited velocity estimation's accuracy [1]. Due to these advantages for both functionalities, using OFDM waveform has become popular in SISO JCAS systems [28]–[30], as well as in MIMO JCAS systems [31]–[33].

In this article, we focus on MIMO JCAS systems with hybrid beamforming architecture [34]. Almost all works in this topic optimize beamforming for communications and sensing. For instance, authors in [35] optimize hybrid beamforming to obtain a trade-off between communication capacity and a well-designed radar beampattern. In [36], beamforming is optimized while minimizing the number of required radio-frequency (RF) chains. The work in [37] optimizes the beamforming to minimize the Cramer–Rao lower bound (CRLB) of direction-of-arrival (DoA) estimate of sensing while guaranteeing some performance of the communication users. However, unlike other works, we optimize the OFDM data streams while having well-designed beampatterns for communications and sensing. Moreover, we demonstrate the methodology to obtain range–velocity and range–angle maps of the environment for MIMO systems with hybrid architecture and spatial multiplexing since the radar processing is not as straightforward as in SISO JCAS systems.

We consider a MIMO transceiver (TRX) that maintains links with users having multiple OFDM data streams over frequency-selective non-line-of-sight (NLoS) channels. Simultaneously, separate OFDM sensing data streams are transmitted to multiple sensing directions. Therefore, some of the communication streams' power is reallocated to the sensing streams. The reflections from the environment due to communications and sensing streams are used to sense the environment through MIMO radar processing, extending our work in [38]. Since the TX signals are essentially communication waveforms, they are not necessarily orthogonal, although they can be considered to be statistically independent.

Moreover, sensing streams are optimized to minimize the CRLBs of DoA and delay estimates jointly. Our earlier work in [4] analyzed a similar problem for a SISO JCAS system with a single stream. In contrast, due to multiple antennas and data streams, TX precoders and RX combiners of the MIMO TRX and different users' RX combiners, affect the waveform optimization. Moreover, they need to be chosen to eliminate the interference evident in MIMO JCAS systems, which are the intra-user and inter-user interference, and sensing streams' interference to communication users (i.e., radar–communications interference). Since multiple TX streams are used for communications and sensing, there is complete flexibility to optimize a TX stream entirely compared to [4], where only a portion of the subcarriers in the TX stream could be optimized. Considering all these changes, we completely revamped the system model and the related formulations when moving from the earlier SISO system to this new MIMO system.

The main contributions of this article can be summarized as follows:

- We derive CRLB expressions for the delay and DoA estimates of sensing for a MIMO-OFDM communications system with hybrid architecture used for JCAS.
- We obtain the analytical solution for joint optimization of the two CRLBs, providing the optimal subcarrier allocation for sensing streams. We also present an algorithm for the task.
- We demonstrate a step-by-step procedure for obtaining the range–angle and range–velocity maps for MIMO systems with multiple TX communication streams when the signals at the MIMO TX elements are not orthogonal.
- We design TX precoders and RX combiners to minimize inter-user, intra-user, and radar-communications interference while facilitating JCAS.
- We apply the proposed beamforming, waveform optimization, and radar processing for a standard-compliant 5G OFDM waveform to evaluate the communications and sensing performance through simulations.

The remainder of the article is organized as follows. Section II discusses the system model of the MIMO JCAS system. Section III describes the proposed range–angle and range–velocity processing, along with the optimization of the TX and RX beamforming. Section IV discusses the optimization scheme to jointly minimize the CRLBs of delay and DoA, which is complemented by including an algorithm. Section V applies the derived solutions to a standard-compliant 5G OFDM waveform through simulations to depict the feasibility of the proposed beamforming, waveform optimization, and radar processing. Finally, Section VI summarizes the article's main conclusions. Furthermore, Appendix A provides the solution to OFDM waveform optimization.

*Notations:* The subscripts $(\cdot)_{\text{TX}}$ and $(\cdot)_{\text{RX}}$ denote the TX and RX, while $(\cdot)_{\text{com}}$ and $(\cdot)_{\text{rad}}$ represent communications and radar, and the superscripts $(\cdot)^{\text{RF}}$ and $(\cdot)^{\text{BB}}$ correspond to components in the RF and baseband (BB) parts of the MIMO TRX. Matrices are represented by bold uppercase letters (i.e., $\mathbf{W}_{\text{TX},m}^{\text{RF}}$), vectors are represented by bold lowercase letters (i.e., $\mathbf{v}_{n,m}$), and scalars are denoted by normal font (i.e., $U_{\text{com}}$); $|\cdot|$ and $\|\cdot\|$ denote the absolute and $l_2$ norm operations, $(\cdot)^T$, $(\cdot)^H$, and $(\cdot)^*$ denote the transpose, Hermitian, and conjugate operations, and $\mathbb{E}\{\cdot\}$, $\det\{\cdot\}$, and $\Re\{\cdot\}$ denote the expectation, determinant, and real operations, respectively.

## II. System Model

A MIMO communications TRX with a hybrid architecture, e.g., a 5G base station, is also used as a radar TRX, as illustrated in Fig. 1. It is assumed that the communications system operates at mm-wave frequencies, in line with the FR2-1 frequency range (24.25–52.60 GHz) [39]. The system maintains links with $U_{\text{com}}$ users having multiple streams over

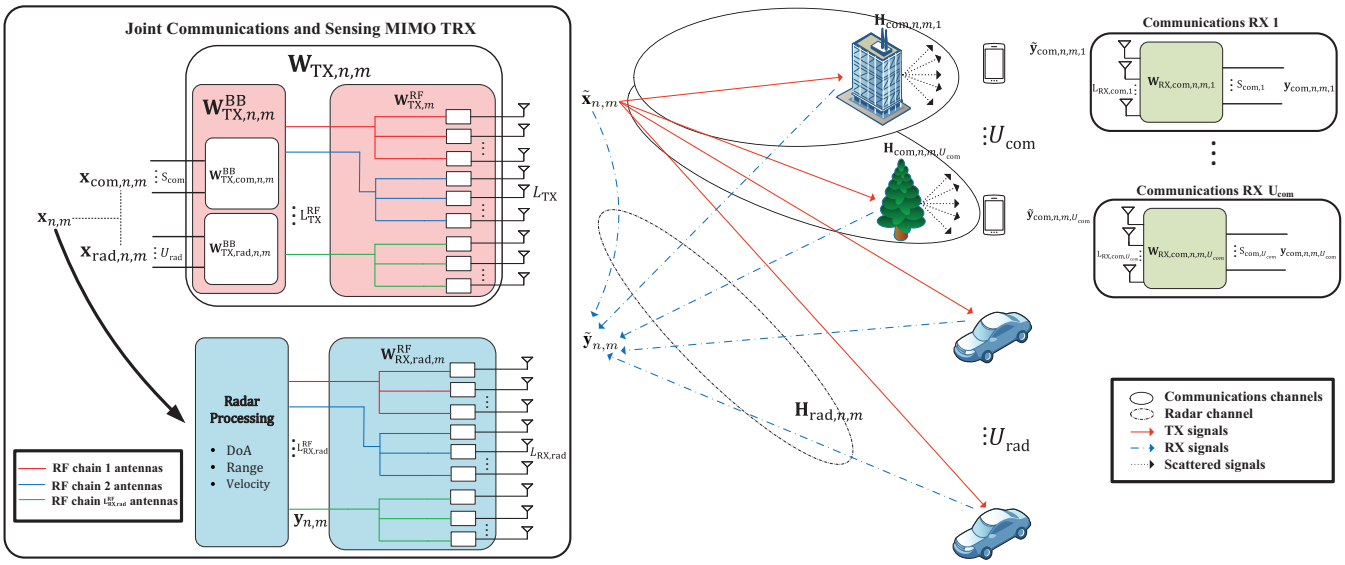


Fig. 1. The considered MIMO-OFDM JCAS system with hybrid architecture where each set of colored lines within $\mathbf{W}^{\text{RF}}_{\text{TX},m}$ and $\mathbf{W}^{\text{RF}}_{\text{RX,rad},m}$ denotes the antennas connected to a particular RF chain. Lines outside the *joint communications and sensing MIMO TRX* correspond to the TX, RX, and scattered signals.

frequency-selective NLoS communications channels while simultaneously sensing the environment through additional $U_{\text{rad}}$ beams, where a different TX stream is used at each sensing direction. In addition, communications, as well as sensing streams, are OFDM waveforms. As depicted in Fig. 1, monostatic sensing is performed, and as such, all spatial streams, i.e., both communications and sensing, can be used for radar processing at the MIMO TRX. Dedicated pilots for sensing are not necessary since the TX streams are completely known at the MIMO RX. The communications RXs also have a hybrid architecture. Table I lists some important parameters for this section.

At MIMO TX side, the number of antenna elements and RF chains are given by $L_{\text{TX}}$ and $L^{\text{RF}}_{\text{TX}}$, with $L^{\text{RF}}_{\text{TX}} \leq L_{\text{TX}}$. Similarly, for MIMO RX side, there are $L_{\text{RX,rad}}$ and $L^{\text{RF}}_{\text{RX,rad}}$ numbers of antennas and RF chains, with $L^{\text{RF}}_{\text{RX,rad}} \leq L_{\text{RX,rad}}$. The $u^{\text{th}}$ communications user has $S_{\text{com},u}$ streams, with $S_{\text{com},u} \geq 1$. Each stream has a time-frequency OFDM grid with $M$ symbols and $N$ active subcarriers. For a given OFDM symbol index $m$ and subcarrier index $n$, the TX frequency-domain symbols' vector of the $u^{\text{th}}$ user is of size $S_{\text{com},u} \times 1$, and given by $\mathbf{x}_{\text{com},n,m,u} = [x_{\text{com},n,m,1}, \cdots, x_{\text{com},n,m,S_{\text{com},u}}]^T$, with $x_{\text{com},n,m,u}$ representing a complex frequency-domain symbol. Here, $n \in [1, N]$, $m \in [1, M]$, and $u \in [1, U_{\text{com}}]$. Symbols for all users are then denoted as $\mathbf{x}_{\text{com},n,m} = [\mathbf{x}^T_{\text{com},n,m,1}, \ldots, \mathbf{x}^T_{\text{com},n,m,U_{\text{com}}}]^T$, which is of size $S_{\text{com}} \times 1$, where $S_{\text{com}}$ is the total number of communications streams. The TX frequency-domain symbols' vector for the sensing streams is given by $\mathbf{x}_{\text{rad},n,m} = [x_{\text{rad},n,m,1}, \ldots, x_{\text{rad},n,m,U_{\text{rad}}}]^T$, of size $U_{\text{rad}} \times 1$. These two vectors for communications and sensing are then combined as $\mathbf{x}_{n,m} = [\mathbf{x}^T_{\text{com},n,m}, \mathbf{x}^T_{\text{rad},n,m}]^T$, where $\mathbf{x}_{n,m}$ is a vector of size $S \times 1$ with $S = S_{\text{com}} + U_{\text{rad}}$. The instantaneous TX powers for communications and sensing data streams are respectively given by

$$P_{\text{com}} = \sum_{m=1}^{M} \sum_{n=1}^{N} \sum_{s=1}^{S_{\text{com}}} |x_{n,m,s}|^2, \tag{1}$$

$$P_{\text{rad}} = \sum_{m=1}^{M} \sum_{n=1}^{N} \sum_{s=S_{\text{com}}+1}^{S} |x_{n,m,s}|^2, \tag{2}$$

where $(\mathbf{x}_{n,m})_s = x_{n,m,s}$ represents the $s^{\text{th}}$ element of $\mathbf{x}_{n,m}$, while $P_{\text{t}} = P_{\text{com}} + P_{\text{rad}}$ denotes the total power of the streams.

It should be noted here that $P_{\text{com}}$ and $P_{\text{rad}}$ are not the physical TX powers from the antenna elements corresponding to communications and sensing; rather they are the total sum of powers of the complex symbols of all the corresponding TX streams. They are necessary for the optimization problem discussed in Section IV. The actual TX power of the considered JCAS system can be calculated based on (4), which depends on the beamforming weights and their normalization, and it is different but roughly proportional to powers in (1) and (2).

The TX baseband weights are frequency/time-dependent, and they are given for communications and sensing as $\mathbf{W}^{\text{BB}}_{\text{TX,com},n,m}$ and $\mathbf{W}^{\text{BB}}_{\text{TX,rad},n,m}$, of sizes $L^{\text{RF}}_{\text{TX}} \times S_{\text{com}}$ and $L^{\text{RF}}_{\text{TX}} \times U_{\text{rad}}$, while

$$\mathbf{W}^{\text{BB}}_{\text{TX,com},n,m} = [\mathbf{W}^{\text{BB}}_{\text{TX,com},n,m,1}, \ldots, \mathbf{W}^{\text{BB}}_{\text{TX,com},n,m,U_{\text{com}}}] \tag{3}$$

consists of all the TX baseband matrices of the communications users. The matrices $\mathbf{W}^{\text{BB}}_{\text{TX,com},n,m}$ and $\mathbf{W}^{\text{BB}}_{\text{TX,rad},n,m}$ are then combined to formulate a single baseband precoder matrix as $\mathbf{W}^{\text{BB}}_{\text{TX},n,m} = [\mathbf{W}^{\text{BB}}_{\text{TX,com},n,m}, \mathbf{W}^{\text{BB}}_{\text{TX,rad},n,m}]$, which is of size $L^{\text{RF}}_{\text{TX}} \times S$. The TX RF weights are time-dependent but frequency-independent, common to all communications and sensing streams for a single OFDM symbol, and are given by the matrix $\mathbf{W}^{\text{RF}}_{\text{TX},m}$, which is of size $L_{\text{TX}} \times L^{\text{RF}}_{\text{TX}}$. Then, the frequency-domain symbols at the TX antenna elements are given by

$$\tilde{\mathbf{x}}_{n,m} = \mathbf{W}^{\text{RF}}_{\text{TX},m} \mathbf{W}^{\text{BB}}_{\text{TX},n,m} \mathbf{x}_{n,m}, \tag{4}$$

where $\tilde{\mathbf{x}}_{n,m}$ is of size $L_{\text{TX}} \times 1$. Additionally, the total TX precoder matrix is represented as

$$\mathbf{W}_{\text{TX},n,m} = \left[\mathbf{W}^{\text{RF}}_{\text{TX},m}\mathbf{W}^{\text{BB}}_{\text{TX,com},n,m}, \mathbf{W}^{\text{RF}}_{\text{TX},m}\mathbf{W}^{\text{BB}}_{\text{TX,rad},n,m}\right], \quad (5)$$

which combines RF and baseband beamforming of communications and sensing. The design of all beamforming matrices is discussed in Section III-B. It should also be noted that the frequencies corresponding to all the $N$ subcarriers are considered to be transmitted by the antennas.

### A. MIMO Radar

As depicted in Fig. 1, the TX signal $\tilde{\mathbf{x}}_{n,m}$ in (4) is reflected from the communications scatterers and radar targets and received back at the MIMO RX. Assuming there are $K_{\text{t}}$ point targets comprising both radar targets and communications scatterers, the RX signal at the MIMO RX can be written as

$$\tilde{\mathbf{y}}_{n,m} = \sum_{k=1}^{K_{\text{t}}} b_k e^{-\jmath 2\pi n \Delta f \tau_k} e^{\jmath 2\pi m \frac{f_{\text{D},k}}{\Delta f}} \mathbf{a}_{\text{RX},n}(\theta_k)\mathbf{a}^H_{\text{TX},n}(\theta_k)\tilde{\mathbf{x}}_{n,m} + \tilde{\mathbf{v}}_{n,m}, \quad (6)$$

where $\tilde{\mathbf{y}}_{n,m}$ and $\tilde{\mathbf{v}}_{n,m}$ are the RX frequency-domain symbols and noise samples of sizes $L_{\text{RX,rad}} \times 1$. The variables $b_k$, $\tau_k$, and $f_{\text{D},k}$ denote the attenuation constant, two-way delay, and Doppler-shift of the $k^{\text{th}}$ target, while angles of departure and arrival, expressed by $\theta_k$, are considered to be the same, assuming distant targets and the TX and RX arrays being closely situated. The TX and RX steering vectors of the $k^{\text{th}}$ target and for the $n^{\text{th}}$ subcarrier are given by $\mathbf{a}_{\text{TX},n}(\theta_k)$ and $\mathbf{a}_{\text{RX},n}(\theta_k)$, while the subcarrier spacing is denoted by $\Delta f$.

For a uniform linear array with $L$ elements and half-wavelength separation, the RX or TX steering vectors, i.e., either $\mathbf{a}_{\text{RX},n}(\theta_k)$ or $\mathbf{a}_{\text{TX},n}(\theta_k)$, can be given generally as

$$\begin{aligned}\mathbf{a}_n(\theta_k) &= \left[1, e^{\jmath\pi \frac{\lambda}{\lambda_n}\sin(\theta_k)}, \ldots, e^{\jmath\pi(L-1)\frac{\lambda}{\lambda_n}\sin(\theta_k)}\right]^T \\ &= \left[1, e^{\jmath\pi \frac{f_{\text{com}}+n\Delta f}{f_{\text{com}}}\sin(\theta_k)}, \ldots, e^{\jmath\pi(L-1)\frac{f_{\text{com}}+n\Delta f}{f_{\text{com}}}\sin(\theta_k)}\right]^T,\end{aligned} \quad (7)$$

where $\lambda$ and $\lambda_n$ are the wavelengths corresponding to the carrier frequency and the $n^{\text{th}}$ subcarrier frequency. Hence, the steering vector changes depending on the frequency of the subcarrier. However, in this article, we focus on a system where the bandwidth w.r.t. the carrier frequency is not high, i.e., $\frac{\lambda}{\lambda_n} = \frac{f_{\text{com}}+n\Delta f}{f_{\text{com}}} \approx 1$, with $f_{\text{com}}$ being the carrier frequency. Hence, the frequency-dependent steering vector in (7) can be simplified as

$$\mathbf{a}(\theta_k) \approx \left[1, e^{\jmath\pi\sin(\theta_k)}, \ldots, e^{\jmath\pi(L-1)\sin(\theta_k)}\right]^T. \quad (8)$$

We will thus use this frequency-independent steering vector throughout the rest of the article for both TX and RX arrays. The approximation in (8) cannot be used for systems where the relative bandwidth w.r.t. the carrier frequency is high, as it can degrade the radar performance, e.g., increase of side-lobes. In such systems, the frequency-dependent steering vector in (7) should be used throughout all concerning equations of this article, e.g., (30) and (31).

TABLE I
SYSTEM MODEL PARAMETERS

| Parameter | Definition | Size |
|---|---|---|
| $U_{\text{com}}$, $U_{\text{rad}}$ | Number of communications users and sensing beams | $1 \times 1$ |
| $L_{\text{TX}}$, $L^{\text{RF}}_{\text{TX}}$ | Number of antenna elements and RF chains of MIMO TX | $1 \times 1$ |
| $L_{\text{RX,rad}}$, $L^{\text{RF}}_{\text{RX,rad}}$ | Number of antenna elements and RF chains of MIMO RX | $1 \times 1$ |
| $M$, $N$ | Number of OFDM symbols and active subcarriers in one TX stream | $1 \times 1$ |
| $\Delta f$ | Subcarrier spacing | $1 \times 1$ |
| $S_{\text{com},u}$ | Number of TX streams of $u^{\text{th}}$ user | $1 \times 1$ |
| $S_{\text{com}}$, $S$ | Number of communications and total streams | $1 \times 1$ |
| $K_{\text{t}}$ | Number of point targets | $1 \times 1$ |
| $\mathbf{x}_{\text{com},n,m}$, $\mathbf{x}_{\text{rad},n,m}$ | TX streams' symbols for communications and sensing | $S_{\text{com}} \times 1$, $U_{\text{rad}} \times 1$ |
| $\mathbf{x}_{n,m}$, $\tilde{\mathbf{x}}_{n,m}$ | TX streams' symbols and symbols at MIMO TX | $S \times 1$, $L_{\text{TX}} \times 1$ |
| $\mathbf{y}_{n,m}$, $\tilde{\mathbf{y}}_{n,m}$ | RX baseband symbols and symbols at MIMO RX | $L^{\text{RF}}_{\text{RX,rad}} \times 1$ $L_{\text{RX,rad}} \times 1$ |
| $\mathbf{y}_{\text{com},n,m}$ | RX streams' symbols of all users | $S_{\text{com}} \times 1$ |
| $\mathbf{W}^{\text{BB}}_{\text{TX,com},n,m}$, $\mathbf{W}^{\text{BB}}_{\text{TX,rad},n,m}$ | TX baseband weights for communications and sensing | $L^{\text{RF}}_{\text{TX}} \times S_{\text{com}}$, $L^{\text{RF}}_{\text{TX}} \times U_{\text{rad}}$ |
| $\mathbf{W}^{\text{BB}}_{\text{TX},n,m}$ | Total TX baseband weights | $L^{\text{RF}}_{\text{TX}} \times S$ |
| $\mathbf{W}^{\text{RF}}_{\text{TX},m}$, $\mathbf{W}^{\text{RF}}_{\text{RX,rad},m}$ | TX and RX RF weights of MIMO TRX | $L_{\text{TX}} \times L^{\text{RF}}_{\text{TX}}$, $L_{\text{RX,rad}} \times L^{\text{RF}}_{\text{RX,rad}}$ |
| $\mathbf{W}_{\text{TX},n,m}$ | Total TX precoder weights | $L_{\text{TX}} \times S$ |
| $\mathbf{W}_{\text{RX,com},n,m,u}$, $\mathbf{W}_{\text{RX,com},n,m}$ | RX combiner of $u^{\text{th}}$/all user/s | $L_{\text{RX,com},u} \times S_{\text{com},u}$, $L_{\text{RX,com}} \times S_{\text{com}}$ |
| $\mathbf{A}_{\text{TX}}(\boldsymbol{\theta})$, $\mathbf{A}_{\text{RX}}(\boldsymbol{\theta})$ | TX and RX steering vectors for all targets | $L_{\text{TX}} \times K_{\text{t}}$, $L_{\text{RX,rad}} \times K_{\text{t}}$ |
| $\mathbf{H}_{\text{rad},n,m}$, $\mathbf{H}_{n,m}$ | Radar channel and effective radar channel | $K_{\text{t}} \times K_{\text{t}}$, $L^{\text{RF}}_{\text{RX,rad}} \times S$ |
| $\mathbf{H}_{\text{com},n,m,u}$, $\mathbf{H}_{\text{com},n,m}$ | Communications channel for $u^{\text{th}}$/all user/s | $L_{\text{RX,com},u} \times L_{\text{TX}}$, $L_{\text{RX,com}} \times L_{\text{TX}}$ |

Converting (6) into matrix notation and applying RX RF combining yields the RX baseband symbols as

$$\mathbf{y}_{n,m} = \underbrace{(\mathbf{W}^{\text{RF}}_{\text{RX,rad},m})^H \mathbf{A}_{\text{RX}}(\boldsymbol{\theta})\mathbf{H}_{\text{rad},n,m}\mathbf{A}^H_{\text{TX}}(\boldsymbol{\theta})\mathbf{W}^{\text{RF}}_{\text{TX},m}\mathbf{W}^{\text{BB}}_{\text{TX},n,m}}_{\mathbf{H}_{n,m}} \cdot \mathbf{x}_{n,m} + \mathbf{v}_{n,m}, \quad (9)$$

where the RX RF combiner $\mathbf{W}^{\text{RF}}_{\text{RX,rad},m}$ that is time-dependent and frequency-independent is of size $L_{\text{RX,rad}} \times L^{\text{RF}}_{\text{RX,rad}}$, $\mathbf{A}_{\text{RX}}(\boldsymbol{\theta}) = [\mathbf{a}_{\text{RX}}(\theta_1), \ldots, \mathbf{a}_{\text{RX}}(\theta_{K_{\text{t}}})]$ is of size $L_{\text{RX,rad}} \times K_{\text{t}}$ and $\mathbf{A}_{\text{TX}}(\boldsymbol{\theta}) = [\mathbf{a}_{\text{TX}}(\theta_1), \ldots, \mathbf{a}_{\text{TX}}(\theta_{K_{\text{t}}})]$ is of size $L_{\text{TX}} \times K_{\text{t}}$. Additionally, $\boldsymbol{\theta} = [\theta_1, \ldots, \theta_{K_{\text{t}}}]^T$ is the vector of all targets' directions, and $\mathbf{H}_{\text{rad},n,m}$ is a diagonal matrix of size $K_{\text{t}} \times K_{\text{t}}$, and it represents the radar channel where $(\mathbf{H}_{\text{rad},n,m})_{k,k} = b_k e^{-\jmath 2\pi n \Delta f \tau_k} e^{\jmath 2\pi m \frac{f_{\text{D},k}}{\Delta f}}$. The vectors $\mathbf{y}_{n,m}$ and $\mathbf{v}_{n,m}$ are of size $L^{\text{RF}}_{\text{RX,rad}} \times 1$. The effective radar channel between the TX streams and RX baseband symbols is given by $\mathbf{H}_{n,m}$, which is of size $L^{\text{RF}}_{\text{RX,rad}} \times S$. Considering different TX streams, (9) can alternatively be written as

$$\mathbf{y}_{n,m} = \underbrace{\left[x_{n,m,1}\mathbf{I}, \ldots, x_{n,m,S}\mathbf{I}\right]}_{\mathbf{X}_{n,m}} \underbrace{\left[\mathbf{h}^T_{n,m,1}, \ldots, \mathbf{h}^T_{n,m,S}\right]^T}_{\mathbf{h}_{n,m}} + \mathbf{v}_{n,m}, \quad (10)$$

where $\mathbf{I}$ is the $L^{\text{RF}}_{\text{RX,rad}} \times L^{\text{RF}}_{\text{RX,rad}}$ identity matrix, $\mathbf{X}_{n,m}$ is of size $L^{\text{RF}}_{\text{RX,rad}} \times (L^{\text{RF}}_{\text{RX,rad}} \cdot S)$, and $\mathbf{h}_{n,m}$ is a vector of size $(L^{\text{RF}}_{\text{RX,rad}} \cdot S) \times 1$, and $\mathbf{h}_{n,m,s} = (\mathbf{H}_{n,m})_s$ denotes $s^{\text{th}}$ column of $\mathbf{H}_{n,m}$, given by

$$\mathbf{h}_{n,m,s} = (\mathbf{W}^{\text{RF}}_{\text{RX,rad},m})^H \mathbf{A}_{\text{RX}}(\boldsymbol{\theta}) \mathbf{H}_{\text{rad},n,m} \cdot \mathbf{A}^H_{\text{TX}}(\boldsymbol{\theta}) \mathbf{W}^{\text{RF}}_{\text{TX},m} (\mathbf{W}^{\text{BB}}_{\text{TX},n,m})_s. \quad (11)$$

The equation in (11) can then be extended by considering multiple OFDM symbols as

$$\underbrace{\begin{bmatrix} \mathbf{y}_{n,1} \\ \mathbf{y}_{n,2} \\ \vdots \\ \mathbf{y}_{n,M} \end{bmatrix}}_{\mathbf{y}_n} = \underbrace{\begin{bmatrix} \mathbf{X}_{n,1} & \mathbf{0} & \dots & \mathbf{0} \\ \mathbf{0} & \mathbf{X}_{n,2} & \dots & \mathbf{0} \\ \vdots & \vdots & \vdots & \vdots \\ \mathbf{0} & \mathbf{0} & \dots & \mathbf{X}_{n,M} \end{bmatrix}}_{\mathbf{X}_n} \underbrace{\begin{bmatrix} \mathbf{h}_{n,1} \\ \mathbf{h}_{n,2} \\ \vdots \\ \mathbf{h}_{n,M} \end{bmatrix}}_{\mathbf{h}_n} + \mathbf{v}_n, \quad (12)$$

where $\mathbf{y}_n$, $\mathbf{X}_n$, $\mathbf{h}_n$, and $\mathbf{v}_n$ are of dimensions $(L^{\text{RF}}_{\text{RX,rad}} \cdot M) \times 1$, $(L^{\text{RF}}_{\text{RX,rad}} \cdot M) \times (L^{\text{RF}}_{\text{RX,rad}} \cdot M \cdot S)$, $(L^{\text{RF}}_{\text{RX,rad}} \cdot M \cdot S) \times 1$, and $(L^{\text{RF}}_{\text{RX,rad}} \cdot M) \times 1$, respectively.

### *B. MIMO Communications RXs*

Each $u^{\text{th}}$ communications user has $L_{\text{RX,com},u}$ RX antennas, and the frequency-domain symbols at the RX antennas for the $m^{\text{th}}$ OFDM symbol and the $n^{\text{th}}$ subcarrier can be written as

$$\begin{aligned} \tilde{\mathbf{y}}_{\text{com},n,m,u} &= \mathbf{H}_{\text{com},n,m,u} \mathbf{W}^{\text{RF}}_{\text{TX},m} \mathbf{W}^{\text{BB}}_{\text{TX,com},n,m,u} \mathbf{x}_{\text{com},n,m,u} \\ &+ \mathbf{H}_{\text{com},n,m,u} \mathbf{W}^{\text{RF}}_{\text{TX},m} \sum_{u' \neq u} \mathbf{W}^{\text{BB}}_{\text{TX,com},n,m,u'} \mathbf{x}_{\text{com},n,m,u'} \\ &+ \mathbf{H}_{\text{com},n,m,u} \mathbf{W}^{\text{RF}}_{\text{TX},m} \mathbf{W}^{\text{BB}}_{\text{TX,rad},n,m} \mathbf{x}_{\text{rad},n,m} + \tilde{\mathbf{v}}_{\text{com},n,m,u}. \end{aligned} \quad (13)$$

Here, the first term corresponds to the RX signal due to $u^{\text{th}}$ user's streams, second term is the inter-user interference, while the third term denotes radar-communications interference. Further, $\mathbf{H}_{\text{com},n,m,u}$ is the channel between the MIMO TX antennas and the $u^{\text{th}}$ user's RX antennas and is of size $L_{\text{RX,com},u} \times L_{\text{TX}}$. It can be given as [40]

$$\mathbf{H}_{\text{com},n,m,u} = \sum_{k=1}^{K_{\text{com},u}} b_{\text{com},u,k} e^{-\jmath 2\pi n \Delta f \tau_{\text{com},u,k}} e^{\jmath 2\pi m \frac{f_{\text{com,D},u,k}}{\Delta f}} \cdot \mathbf{a}_{\text{RX},u}(\theta'_{\text{com},u,k}) \mathbf{a}^H_{\text{TX}}(\theta_{\text{com},u,k}), \quad (14)$$

where $K_{\text{com},u}$ is the total number of point scatterers considered for the $u^{\text{th}}$ user, $b_{\text{com},u,k}$, $\tau_{\text{com},u,k}$, and $f_{\text{com,D},u,k}$ denote the attenuation constant, one-way delay and Doppler-shift of the $k^{\text{th}}$ scatterer, respectively. The angles of departure and arrival are given by $\theta_{\text{com},u,k}$ and $\theta'_{\text{com},u,k}$, while $\mathbf{a}_{\text{RX},u}(\theta)$ represents the RX steering vector of the $u^{\text{th}}$ user. In addition, it is also assumed that the MIMO TX knows the best angle for signal transmission for each user.

The RX baseband symbols are then given after applying RX combining to (13) as

$$\begin{aligned} \mathbf{y}_{\text{com},n,m,u} &= (\mathbf{W}_{\text{RX,com},n,m,u})^H \mathbf{H}_{\text{com},n,m,u} \mathbf{W}^{\text{RF}}_{\text{TX},m} \mathbf{W}^{\text{BB}}_{\text{TX,com},n,m,u} \\ &\cdot \mathbf{x}_{\text{com},n,m,u} + (\mathbf{W}_{\text{RX,com},n,m,u})^H \mathbf{H}_{\text{com},n,m,u} \mathbf{W}^{\text{RF}}_{\text{TX},m} \\ &\cdot \sum_{u' \neq u} \mathbf{W}^{\text{BB}}_{\text{TX,com},n,m,u'} \mathbf{x}_{\text{com},n,m,u'} + (\mathbf{W}_{\text{RX,com},n,m,u})^H \\ &\cdot \mathbf{H}_{\text{com},n,m,u} \mathbf{W}^{\text{RF}}_{\text{TX},m} \mathbf{W}^{\text{BB}}_{\text{TX,rad},n,m} \mathbf{x}_{\text{rad},n,m} + \mathbf{v}_{\text{com},n,m,u}, \end{aligned} \quad (15)$$

where $\mathbf{y}_{\text{com},n,m,u}$ and $\mathbf{v}_{\text{com},n,m,u}$ are vectors of size $S_{\text{com},u} \times 1$. In addition, $\mathbf{v}_{\text{com},n,m,u} = (\mathbf{W}_{\text{RX,com},n,m,u})^H \tilde{\mathbf{v}}_{\text{com},n,m,u}$. The RX combiner for the $u^{\text{th}}$ user is given by $\mathbf{W}_{\text{RX,com},n,m,u}$ that is frequency/time-dependent. The frequency-domain symbols of all users' streams can then be represented as

$$\begin{aligned} \mathbf{y}_{\text{com},n,m} &= (\mathbf{W}_{\text{RX,com},n,m})^H \mathbf{H}_{\text{com},n,m} \mathbf{W}^{\text{RF}}_{\text{TX},m} \mathbf{W}^{\text{BB}}_{\text{TX,com},n,m} \\ &\cdot \mathbf{x}_{\text{com},n,m} + (\mathbf{W}_{\text{RX,com},n,m})^H \mathbf{H}_{\text{com},n,m} \\ &\cdot \mathbf{W}^{\text{RF}}_{\text{TX},m} \mathbf{W}^{\text{BB}}_{\text{TX,rad},n,m} \mathbf{x}_{\text{rad},n,m} + \mathbf{v}_{\text{com},n,m}, \end{aligned} \quad (16)$$

where the first and second terms in (15) are combined to formulate the first term in (16), and

$$\mathbf{W}_{\text{RX,com},n,m} = \begin{bmatrix} \mathbf{W}_{\text{RX,com},n,m,1} & \dots & \mathbf{0} \\ \vdots & \vdots & \vdots \\ \mathbf{0} & \dots & \mathbf{W}_{\text{RX,com},n,m,U_{\text{com}}} \end{bmatrix}, \quad (17)$$

which is of size $L_{\text{RX,com}} \times S_{\text{com}}$, $\mathbf{H}_{\text{com},n,m} = [\mathbf{H}^T_{\text{com},n,m,1}, \dots, \mathbf{H}^T_{\text{com},n,m,U_{\text{com}}}]^T$ is of size $L_{\text{RX,com}} \times L_{\text{TX}}$, $\mathbf{y}_{\text{com},n,m}$ is of size $S_{\text{com}} \times 1$, and $\mathbf{v}_{\text{com},n,m}$ is of size $S_{\text{com}} \times 1$. Here, $L_{\text{RX,com}} = \sum_{u=1}^{U_{\text{com}}} L_{\text{RX,com},u}$.

The communication performance of the system is generally evaluated through the channel capacity. For calculating it, covariance matrices of the different terms in (15) need to be calculated, which are the signal-of-interest (SOI), inter-user interference and radar–communications interference, respectively, in the first, second, and third terms. These are derived next, where we have used the substitution $\tilde{\mathbf{H}}_{\text{com},n,m,u} = (\mathbf{W}_{\text{RX,com},n,m,u})^H \mathbf{H}_{\text{com},n,m,u} \mathbf{W}^{\text{RF}}_{\text{TX},m}$ since it is common to the first three terms.

The covariance matrix of SOI is first given by

$$\mathbf{R}_{\text{SOI},n,m,u} = \tilde{\mathbf{H}}_{\text{com},n,m,u} \mathbf{W}^{\text{BB}}_{\text{TX,com},n,m} \mathbf{Q}_{\text{SOI},n,m,u} \cdot (\mathbf{W}^{\text{BB}}_{\text{TX,com},n,m})^H \tilde{\mathbf{H}}^H_{\text{com},n,m,u}, \quad (18)$$

where $\mathbf{Q}_{\text{SOI},n,m,u} = \mathbb{E}\{\mathbf{x}_{\text{com},n,m,u} \mathbf{x}^H_{\text{com},n,m,u}\}$. Next, the covariance matrix of inter-user interference is given by

$$\mathbf{R}_{\text{int,com},n,m,u} = \tilde{\mathbf{H}}_{\text{com},n,m,u} \mathbf{Q}_{\text{int,com},n,m,u} \tilde{\mathbf{H}}^H_{\text{com},n,m,u}, \quad (19)$$

where

$$\mathbf{Q}_{\text{int,com},n,m,u} = \mathbb{E}\Big\{ \Big( \sum_{u' \neq u} \mathbf{W}^{\text{BB}}_{\text{TX,com},n,m,u'} \mathbf{x}_{\text{com},n,m,u'} \Big) \cdot \Big( \sum_{u' \neq u} \mathbf{W}^{\text{BB}}_{\text{TX,com},n,m,u'} \mathbf{x}_{\text{com},n,m,u'} \Big)^H \Big\}. \quad (20)$$

The covariance matrix of radar–communications interference is then given by

$$\mathbf{R}_{\text{int,rad},n,m,u} = \tilde{\mathbf{H}}_{\text{com},n,m,u} \mathbf{W}^{\text{BB}}_{\text{TX,rad},n,m} \mathbf{Q}_{\text{int,rad},n,m} \cdot (\mathbf{W}^{\text{BB}}_{\text{TX,rad},n,m})^H \tilde{\mathbf{H}}^H_{\text{com},n,m,u}, \quad (21)$$

where $\mathbf{Q}_{\text{int,rad},n,m} = \mathbb{E}\{\mathbf{x}_{\text{rad},n,m} \mathbf{x}^H_{\text{rad},n,m}\}$. Finally, the sum channel capacity of all users for a given channel realization can be written as

$$\zeta_{\text{int,com}} = \sum_{u=1}^{U_{\text{com}}} \sum_{m=1}^{M} \sum_{n=1}^{N} \log_2 \det\big\{ \mathbf{I} + \big( \mathbf{R}_{\text{int,com},n,m,u} + \mathbf{R}_{\text{int,rad},n,m,u} + \sigma^2_u \mathbf{I} \big)^{-1} \mathbf{R}_{\text{SOI},n,m,u} \big\}, \quad (22)$$

where $\sigma_u^2$ is the noise variance at the $u^{\text{th}}$ user. In addition, when only conventional communication is performed, i.e., without JCAS, the sum channel capacity is given as

$$\bar{\zeta}_{\text{com}} = \sum_{u=1}^{U_{\text{com}}} \sum_{m=1}^{M} \sum_{n=1}^{N} \log_2 \det\big\{\mathbf{I} + \big(\bar{\mathbf{R}}_{\text{int,com},n,m,u} + \sigma_u^2\mathbf{I}\big)^{-1}\bar{\mathbf{R}}_{\text{SOI},n,m,u}\big\}, \quad (23)$$

where $\bar{\mathbf{R}}_{\text{int,com},n,m,u}$ and $\bar{\mathbf{R}}_{\text{SOI},n,m,u}$ are the corresponding covariance matrices when only communication is performed.

## III. Radar Processing and Beamforming Design

This section discusses the procedure adopted in obtaining the range–velocity and range–angle maps. First, the range profiles corresponding to the different OFDM symbols are calculated. They are then separately used for calculating the range–velocity and range–angle maps. Next, we describe the design of TX precoders and RX combiners to cancel the inter-user, intra-user, and radar-communications interference.

### A. Derivation of Range–Velocity and Range–Angle Maps

*1) Range-Profile Processing:* The effective radar channel in (9) needs to be estimated to find the range, velocity, and DoA of the targets. As the first step in this process, $\mathbf{h}_n$ in (12) is estimated by applying the least-squares solution as

$$\hat{\mathbf{h}}_n = \mathbf{X}_n^{\dagger}\mathbf{y}_n = \mathbf{h}_n + \Delta\mathbf{h}_n, \quad (24)$$

where $\hat{\mathbf{h}}_n$ is the estimated vector of the same size as $\mathbf{h}_n$, $\Delta\mathbf{h}_n$ is the estimation error vector, and $(\cdot)^{\dagger}$ is the pseudo-inverse operation, respectively. Similar to in (12), $\hat{\mathbf{h}}_n$ can be written as $\hat{\mathbf{h}}_n = [(\hat{\mathbf{h}}_{n,1})^T, \ldots, (\hat{\mathbf{h}}_{n,M})^T]^T$. Similar to in (11), effective radar channel for the $m^{\text{th}}$ OFDM symbol can be written for all streams as $\hat{\mathbf{h}}_{n,m} = [(\hat{\mathbf{h}}_{n,m,1})^T, \ldots, (\hat{\mathbf{h}}_{n,m,S})^T]^T$. Hence, the effective radar channel for $m^{\text{th}}$ OFDM symbol and $s^{\text{th}}$ stream is estimated, which can further be written similarly to (24) as

$$\hat{\mathbf{h}}_{n,m,s} = \mathbf{h}_{n,m,s} + \Delta\mathbf{h}_{n,m,s}, \quad (25)$$

where $\hat{\mathbf{h}}_{n,m,s}$ is of size $L^{\text{RF}}_{\text{RX,rad}} \times 1$. For a SISO system, the range profile is estimated by applying the inverse DFT (IDFT) to the estimated channel [30]. Adopting a similar approach for the MIMO case, $L^{\text{RF}}_{\text{RX,rad}}$ values (across RX RF chains) can be calculated for the $i^{\text{th}}$ range bin by applying IDFT to $\hat{\mathbf{h}}_{n,m,s}$ as

$$\mathbf{d}_{i,m,s} = \sum_{n=1}^{N} q_{i,n}\hat{\mathbf{h}}_{n,m,s} = \Big[\hat{\mathbf{h}}_{1,m,s}, \ldots, \hat{\mathbf{h}}_{N,m,s}\Big]\,\mathbf{q}_i, \quad (26)$$

where $i \in [1, N]$ and $\mathbf{q}_i$ is the IDFT vector of size $N \times 1$, and each element of it is given by $(\mathbf{q}_i)_n = q_{i,n} = e^{\frac{\jmath 2\pi ni}{N}}$, while $\mathbf{d}_{i,m,s}$ is a vector of size $L^{\text{RF}}_{\text{RX,rad}} \times 1$. In addition, the delay of each target is discretized as $\tau_i = \frac{i}{N\Delta f}$.

*2) Range–Velocity Maps:* A DFT is next applied for $\mathbf{d}_{i,m,s}$ to obtain the $(i,j)^{\text{th}}$ element of the range–velocity map as

$$\mathbf{f}_{i,j,s} = \sum_{m=1}^{M} q'_{j,m}\mathbf{d}_{i,m,s} = [\mathbf{d}_{i,1,s}, \ldots, \mathbf{d}_{i,M,s}]\,\mathbf{q}'_j, \quad (27)$$

where $j \in [1, M]$ and $\mathbf{q}'_j$ is the DFT vector of size $M \times 1$, and each element of it is given by $(\mathbf{q}'_j)_m = q'_{j,m} = e^{\frac{\jmath 2\pi mj}{M}}$, while $\mathbf{f}_{i,j,s}$ is a vector of size $L^{\text{RF}}_{\text{RX,rad}} \times 1$. Additionally, the Doppler-shift of each target is discretized as $f_{\text{D},j} = \frac{j\Delta f}{M}$.

*3) Range–Angle Maps:* For calculating the angle profiles, the covariance matrix of the range bin values across different RF chains is needed. Hence, this will be first calculated based on (26), similar to [38] as

$$\mathbf{R}_{i,m,s} = \mathbb{E}\{\mathbf{d}_{i,m,s}\mathbf{d}_{i,m,s}^H\} = \sum_{n_1=1}^{N}\sum_{n_2=1}^{N} q_{i,n_1}q_{i,n_2}^*\mathbf{h}_{n_1,m,s}\mathbf{h}_{n_2,m,s}^H + \sigma^2\mathbf{I}, \quad (28)$$

where $\sigma^2\mathbf{I}$ represents the covariance matrix stemming from the estimation error vector, and it is given by $\sigma^2\mathbf{I} = \sum_{n_1=1}^{N}\sum_{n_2=1}^{N} q_{i,n_1}q_{i,n_2}^*\mathbb{E}\{\Delta\mathbf{h}_{n_1,m,s}\Delta\mathbf{h}_{n_2,m,s}^H\}$. Using (11), (28) can be rewritten in the format

$$\mathbf{R}_{i,m,s} = \mathbf{A}^{\text{RF}}(\boldsymbol{\theta})\bar{\mathbf{R}}_{i,m,s}\mathbf{A}_{\text{RF}}^H(\boldsymbol{\theta}) + \sigma^2\mathbf{I}, \quad (29)$$

where $\mathbf{A}^{\text{RF}}(\boldsymbol{\theta}) = (\mathbf{W}^{\text{RF}}_{\text{RX,rad},m})^H\mathbf{A}_{\text{RX}}(\boldsymbol{\theta})$ is of size $L^{\text{RF}}_{\text{RX,rad}} \times K_{\text{t}}$. Additionally, $\bar{\mathbf{R}}_{i,m,s}$ is the covariance matrix corresponding to the residual terms apart from $(\mathbf{W}^{\text{RF}}_{\text{RX,rad},m})^H\mathbf{A}_{\text{RX}}(\boldsymbol{\theta})$ in $\mathbf{h}_{n,m,s}$ (11). The number of targets $K_{\text{t}}$ can be estimated, for example, using minimum description length method [41] or from the Gerschgorin disk estimator method described in [42]. Using a similar representation of (29) in [38], the (MUltiple SIgnal Classification) MUSIC pseudo-spectrum of the $i^{\text{th}}$ range bin and the $m^{\text{th}}$ OFDM symbol for the $s^{\text{th}}$ stream can be obtained as

$$P(\theta)_{i,m,s} = \frac{1}{\tilde{\mathbf{a}}^H(\theta)\boldsymbol{\Gamma}_{i,m,s}\boldsymbol{\Gamma}_{i,m,s}^H\tilde{\mathbf{a}}(\theta)}, \quad (30)$$

where $\boldsymbol{\Gamma}_{i,m,s} = [\boldsymbol{\gamma}_{i,m,s,1}, \ldots, \boldsymbol{\gamma}_{i,m,s,L^{\text{RF}}_{\text{RX,rad}}-K_{\text{t}}}]$ contains the eigenvectors of $\mathbf{R}_{i,m,s}$ corresponding to the lowest $(L^{\text{RF}}_{\text{RX,rad}} - K_{\text{t}})$ eigenvalues, $\theta = [-90°, 90°]$, and $\tilde{\mathbf{a}}(\theta) = (\mathbf{W}^{\text{RF}}_{\text{RX,rad},m})^H\mathbf{a}_{\text{RX}}(\theta)$, and it represents the effective steering vector at the RX by considering the RX RF beamforming matrix. This is performed for all $i$ values to obtain the range—angle map corresponding to each TX stream and OFDM symbol. In practice, an approximation is used for $\mathbf{R}_{i,m,s}$ as $\mathbf{R}_{i,m,s} \approx \mathbf{d}_{i,m,s}\mathbf{d}_{i,m,s}^H$, instead of the expectation.

Since $\mathbf{R}_{i,m,s}$ is of size $L^{\text{RF}}_{\text{RX,rad}} \times L^{\text{RF}}_{\text{RX,rad}}$, the number of targets that can be reliably detected is given by $L^{\text{RF}}_{\text{RX,rad}} - 1$. In addition, the number of samples needed for range–angle map calculation is given by $(L^{\text{RF}}_{\text{RX,rad}})^2NMS$. Hence, while the increase of $L^{\text{RF}}_{\text{RX,rad}}$ increases the number of targets that can be detected, it also increases the complexity of range–angle map calculation, indicating the trade-off between performance and complexity.

From (30), $S$ streams will produce that many different range–angle maps for a single OFDM symbol due to $\mathbf{W}^{\text{BB}}_{\text{TX},n,m}$ having disparate weights for the TX streams. However, a single

map can be acquired through maximum-ratio combining. For the $s^{\text{th}}$ TX stream, the angle-dependent complex coefficient of the beam pattern can be calculated as $g_{\text{TX},n,m,s}(\theta) = \mathbf{a}_T^H(\theta)\mathbf{W}_{\text{TX},m}^{\text{RF}}(\mathbf{W}_{\text{TX},n,m}^{\text{BB}})_s$. Thus, the combined range–angle map for the $m^{\text{th}}$ OFDM symbol can be written as

$$P(\theta)_{i,m} = \sum_{s=1}^{S} \frac{|g_{\text{TX},n,m,s}(\theta)|^2}{\tilde{\mathbf{a}}^H(\theta)\mathbf{\Gamma}_{i,m,s}\mathbf{\Gamma}_{i,m,s}^H\tilde{\mathbf{a}}(\theta)}. \tag{31}$$

In addition, once the range–angle and range–velocity maps are obtained, additional radar processing is required to detect targets and estimate their parameters, i.e., range, velocity, and angle. Successive maps at different time instants and tracking can also be utilized for this purpose. Once the maps are obtained, detection and estimation can be applied to them [43], [44], but we do not discuss it here in the article.

### *B. Beamforming Design*

This section describes the formulation of different TX and RX beamforming matrices used in this article, and they are designed prior to waveform optimization per Section IV. Hence, any other beamforming design can be used, separate from the one discussed here, and the proposed waveform optimization and radar processing are applicable regardless. It is assumed that users' communications channels are first estimated using reference signals in the downlink and fed back to the MIMO TRX in the uplink; hence this information is assumed to be known.

*1) TX RF Beamforming:* We assume that MIMO TX knows the best TX directions for different users' signals, for $m^{\text{th}}$ OFDM symbol, denoted by $\boldsymbol{\theta}_{\text{com},m} = [\theta_{\text{com},m,1}, \ldots, \theta_{\text{com},m,u}, \ldots, \theta_{\text{com},m,U_{\text{com}}}]^T$, of size $U_{\text{com}} \times 1$. Similarly, sensing directions can be written as $\boldsymbol{\theta}_{\text{rad},m} = [\theta_{\text{rad},m,1}, \ldots, \theta_{\text{rad},m,U_{\text{rad}}}]^T$. All these angles can be denoted as

$$\boldsymbol{\theta}_{\text{TX},m} = [\boldsymbol{\theta}_{\text{com},m}^T, \boldsymbol{\theta}_{\text{rad},m}^T]^T, \tag{32}$$

which is of size $(U_{\text{com}} + U_{\text{rad}}) \times 1$. Then, the beamforming weights for each TX RF chain are obtained with the spatial matched-filter (MF) response to maximize the gains of the RF beampattern at all directions in (32), assuming that the amplitudes and phases of the TX RF beamformer can be modified. These weights are the given as

$$\mathbf{w}_{\text{TX},l_{\text{TX}},m,i}^{\text{RF}} = \begin{cases} \rho \frac{\mathbf{a}_{\text{TX},l_{\text{TX}}}^*(\theta_{\text{TX},m,i})}{||\mathbf{a}_{\text{TX},l_{\text{TX}}}(\theta_{\text{TX},m,i})||}, & \theta_{\text{TX},m,i} \in \boldsymbol{\theta}_{\text{com},m} \\ (1-\rho)\frac{\mathbf{a}_{\text{TX},l_{\text{TX}}}^*(\theta_{\text{TX},m,i})}{||\mathbf{a}_{\text{TX},l_{\text{TX}}}(\theta_{\text{TX},m,i})||}, & \theta_{\text{TX},m,i} \in \boldsymbol{\theta}_{\text{rad},m}, \end{cases} \tag{33}$$

where $i \in [1, (U_{\text{com}} + U_{\text{rad}})]$, $l_{\text{TX}}$ denotes the RF chain index with $l_{\text{TX}} \in [1, L_{\text{TX}}^{\text{RF}}]$, and $\mathbf{a}_{\text{TX},l_{\text{TX}}}(\theta_{\text{TX},m,i})$ is the corresponding TX steering vector specific to the $l_{\text{TX}}^{\text{th}}$ RF chain. Here, $\rho \in [0,1]$, controls the gains between communications and sensing directions. The expression in (33) corresponds to the MF weights to obtain a maximum in the RF beampattern for the $i^{\text{th}}$ angle. However, there should be maximums for all angles, i.e., communications and radar directions. Hence, the weights for all the different angles are summed up to derive the total weights for each RF chain, similar to [45] as

$$\mathbf{w}_{\text{TX},l_{\text{TX}},m}^{\text{RF}} = \sum_{i=1}^{U_{\text{com}}+U_{\text{rad}}} \mathbf{w}_{\text{TX},l_{\text{TX}},m,i}^{\text{RF}}. \tag{34}$$

The RF precoder matrix is then given by stacking the weights for the different RF chains as $\mathbf{W}_{\text{TX},m}^{\text{RF}} = \left[\frac{\mathbf{w}_{\text{TX},1,m}^{\text{RF}}}{\|\mathbf{w}_{\text{TX},1,m}^{\text{RF}}\|}, \ldots, \frac{\mathbf{w}_{\text{TX},L_{\text{TX}}^{\text{RF}},m}^{\text{RF}}}{\|\mathbf{w}_{\text{TX},L_{\text{TX}}^{\text{RF}},m}^{\text{RF}}\|}\right]$, where each column is normalized.

*2) Communication TX baseband and RX Beamforming:* Next, $\mathbf{W}_{\text{TX,com},n,m}^{\text{BB}}$ and $\mathbf{W}_{\text{RX,com},n,m}$ are found using the block diagonalization (BD) method [19]. For this, communication users' channels apart from the $u^{\text{th}}$ user are denoted by

$$\begin{aligned}\bar{\mathbf{H}}_{\text{com},n,m,u} = &[\mathbf{H}_{\text{com},n,m,1}^T\mathbf{W}_{\text{TX},m}^{\text{RF}}, \mathbf{H}_{\text{com},n,m,u-1}^T\mathbf{W}_{\text{TX},m}^{\text{RF}}, \\ &\mathbf{H}_{\text{com},n,m,u+1}^T\mathbf{W}_{\text{TX},m}^{\text{RF}} \cdots, \mathbf{H}_{\text{com},n,m,U_{\text{com}}}^T\mathbf{W}_{\text{TX},m}^{\text{RF}}]^T.\end{aligned} \tag{35}$$

To prevent $u^{\text{th}}$ user interfering other users (inter–user interference), its baseband beamforming matrix $\mathbf{W}_{\text{TX,com},n,m,u}^{\text{BB}}$, as in (3), needs to be in the null-space of $\bar{\mathbf{H}}_{\text{com},n,m,u}$. This is calculated by the singular value decomposition (SVD) of $\bar{\mathbf{H}}_{\text{com},n,m,u}$ and given by

$$\bar{\mathbf{H}}_{\text{com},n,m,u} = \bar{\mathbf{V}}_{\text{left},u}\bar{\mathbf{\Sigma}}_u\left(\bar{\mathbf{V}}_{\text{right},u}^{(1)}, \bar{\mathbf{V}}_{\text{right},u}^{(0)}\right)^H, \tag{36}$$

where $\bar{\mathbf{V}}_{\text{left},u}$ contains the left singular vectors while $\bar{\mathbf{V}}_{\text{right},u}^{(1)}$ and $\bar{\mathbf{V}}_{\text{right},u}^{(0)}$ contain the right singular vectors for non-zero and zero singular values, respectively. In addition, $\mathbf{\Sigma}_u$ is a diagonal matrix containing the singular values. The matrix $\bar{\mathbf{V}}_{\text{right},u}^{(0)}$ corresponds to the basis of the null-space of $\bar{\mathbf{H}}_{\text{com},n,m,u}$. Due to this, columns of $\bar{\mathbf{V}}_{\text{right},u}^{(0)}$ are possible vectors for $\mathbf{W}_{\text{TX,com},n,m,u}^{\text{BB}}$.

For $u^{\text{th}}$ user, $\mathbf{H}_{\text{com},n,m,u}\mathbf{W}_{\text{TX},m}^{\text{RF}}\bar{\mathbf{V}}_{\text{right},u}^{(0)}$ thus represents the effective channel after the inter-user interference is canceled. Its SVD can be represented in a similar format to (36) as

$$\mathbf{H}_{\text{com},n,m,u}\mathbf{W}_{\text{TX},m}^{\text{RF}}\bar{\mathbf{V}}_{\text{right},u}^{(0)} = \mathbf{V}_{\text{left},u}\mathbf{\Sigma}_u\left(\mathbf{V}_{\text{right},u}^{(1)}, \mathbf{V}_{\text{right},u}^{(0)}\right)^H. \tag{37}$$

Finally, TX baseband precoding matrix of the $u^{\text{th}}$ user is selected as $\mathbf{W}_{\text{TX,com},n,m,u}^{\text{BB}} = \bar{\mathbf{V}}_{\text{right},u}^{(0)}\mathbf{V}_{\text{right},u}^{(1)}$, while the RX combiner is chosen as $\mathbf{W}_{\text{RX,com},n,m,u} = \mathbf{V}_{\text{left},u}^H$, ensuring inter-user and intra-user interference are perfectly canceled [46]. This process is performed for all users to obtain $\mathbf{W}_{\text{TX,com},n,m}^{\text{BB}}$ and $\mathbf{W}_{\text{RX,com},n,m}$.

*3) Radar TX Baseband and RX RF Beamforming:* Next, $\mathbf{W}_{\text{TX,rad},n,m}^{\text{BB}}$ is designed to prevent radar–communications interference. For this, second term in (16) needs to be canceled, in which $\mathbf{W}_{\text{TX,rad},n,m}^{\text{BB}}$ has to obey

$$\underbrace{(\mathbf{W}_{\text{RX,com},n,m})^H\mathbf{H}_{\text{com},n,m}\mathbf{W}_{\text{TX},m}^{\text{RF}}}_{\mathbf{Z}_{n,m}}\mathbf{W}_{\text{TX,rad},n,m}^{\text{BB}} = \mathbf{0}, \tag{38}$$

where $\mathbf{0}$ is a matrix of zeros. The baseband precoder for each sensing beam is then designed such that it satisfies (38) while also maximizing the gain at $\theta_{\text{rad},m,u'}$. The solution for this

**Algorithm 1** Design of TX precoders and RX combiners

1: Set the weights for each TX RF chain $\mathbf{w}^{\text{RF}}_{\text{TX},l_{\text{TX}},m}$ such that they maximize TX RF beampattern gains in communication and radar directions, using (33) and (34)
2: Set $\mathbf{W}^{\text{RF}}_{\text{TX},m}$ by stacking normalized $\mathbf{w}^{\text{RF}}_{\text{TX},l_{\text{TX}},m}$ vectors of different RF chains for $l_{\text{TX}} \in [1, L_{\text{TX}}]$
3: Set the TX baseband weights and RX combiner weights of the $u^{\text{th}}$ communication user, $\mathbf{W}^{\text{BB}}_{\text{TX,com},n,m,u}$ and $\mathbf{W}_{\text{RX,com},n,m,u}$, using the BD method in (35)–(37)
4: Stack the different users' TX baseband weights and RX combiners to obtain $\mathbf{W}^{\text{BB}}_{\text{TX,com},n,m}$ and $\mathbf{W}_{\text{RX,com},n,m}$
5: Set the TX baseband precoder of each sensing beam $\mathbf{w}^{\text{BB}}_{\text{TX},n,m,u'}$ such that it maximizes the effective TX beampattern gain in the specific sensing direction while also canceling radar–communication interference, using (39)
6: Set $\mathbf{W}^{\text{RF}}_{\text{RX,rad},m}$ by stacking normalized $\mathbf{w}^{\text{RF}}_{\text{RX,rad},l_{\text{RX}},m}$ vectors of the different RF chains, using (40) and (41)

can be given in a closed form by using the MF and null-space projection methods as [20]

$$\mathbf{w}^{\text{BB}}_{\text{TX,rad},n,m,u'} = \frac{\left(\mathbf{I} - \mathbf{Z}^{\dagger}_{n,m}\mathbf{Z}_{n,m}\right)(\mathbf{W}^{\text{RF}}_{\text{TX},m})^H \mathbf{a}_{\text{TX}}(\theta_{\text{rad},m,u'})}{||(\mathbf{W}^{\text{RF}}_{\text{TX},m})^H \mathbf{a}_{\text{TX}}(\theta_{\text{rad},m,u'})||}. \tag{39}$$

Hence, the baseband weights for radar streams are given by stacking the different sensing beams' baseband precoders as $\mathbf{W}^{\text{BB}}_{\text{TX,rad},n,m} = \left[\frac{\mathbf{w}^{\text{BB}}_{\text{TX,rad},n,m,1}}{\|\mathbf{w}^{\text{BB}}_{\text{TX,rad},n,m,1}\|}, \ldots, \frac{\mathbf{w}^{\text{BB}}_{\text{TX,rad},n,m,U_{\text{rad}}}}{\|\mathbf{w}^{\text{BB}}_{\text{TX,rad},n,m,U_{\text{rad}}}\|}\right]$.

For the MIMO RX, an MF approach is used to receive reflections from different sensing directions. The weights for the $l^{\text{th}}_{\text{RX}}$ RF chain and for the $u'^{\text{th}}$ sensing angle are given by

$$\mathbf{w}^{\text{RF}}_{\text{RX,rad},l_{\text{RX}},m,u'} = \frac{\mathbf{a}^{*}_{\text{RX},l_{\text{RX}}}(\theta_{\text{rad},m,u'})}{||\mathbf{a}_{\text{RX},l_{\text{RX}}}(\theta_{\text{rad},m,u'})||}, \tag{40}$$

where $l_{\text{RX}} \in [1, L^{\text{RF}}_{\text{RX,rad}}]$, while $\mathbf{a}_{\text{RX},l_{\text{RX}}}(\theta_{\text{rad},m,u'})$ is the RX steering vector for $l^{\text{th}}_{\text{RX}}$ RF chain. Combining weights for the different sensing angles leads to RF weights for the $l^{\text{th}}_{\text{RX}}$ RF chain as

$$\mathbf{w}^{\text{RF}}_{\text{RX,rad},l_{\text{RX}},m} = \sum_{u'=1}^{U_{\text{rad}}} \mathbf{w}^{\text{RF}}_{\text{RX,rad},l_{\text{RX}},m,u'}. \tag{41}$$

We here also assume that the RX RF beamformer's amplitudes and phases can be fully controlled, similar to that of the TX RF beamformer. Finally, the RX RF combiner for all the RF chains is given by $\mathbf{W}^{\text{RF}}_{\text{RX,rad},m} = \left[\frac{\mathbf{w}_{\text{RX,rad},1,m}}{\|\mathbf{w}_{\text{RX,rad},1,m}\|}, \ldots, \frac{\mathbf{w}_{\text{RX,rad},L^{\text{RF}}_{\text{RX,rad}},m}}{\|\mathbf{w}_{\text{RX,rad},L^{\text{RF}}_{\text{RX,rad}},m}\|}\right]$, where $\mathbf{W}^{\text{RF}}_{\text{RX,rad},m}$ is of size $L_{\text{RX,rad}} \times L^{\text{RF}}_{\text{RX,rad}}$. Finally, Algorithm 1 indicates the full beamforming design.

## IV. Sensing Waveform Optimization

In this section, we discuss the optimization of subcarrier indices and frequency-domain samples of sensing streams $\mathbf{x}_{\text{rad},n,m}$ to minimize the CRLBs of delay and DoA estimates of sensing, i.e., $\hat{\tau}$ and $\hat{\theta}$, respectively. Here, the CRLB expressions necessary for this section are derived, the related optimization problem is discussed, and the solution is analytically derived. An algorithm is also presented for finding the subcarrier allocation in the sensing streams. Table II lists the important parameters of this section.

### A. CRLB Expressions for the MIMO-OFDM Model

Here, the CRLB expressions for the estimated delay and DoA parameters are derived using the Fisher information matrix $\mathcal{I}(\boldsymbol{\alpha})$ of size $2 \times 2$, where $\boldsymbol{\alpha} = [\theta, \tau]^T$. For this, $\mathbf{v}_n$ in (12) is considered to be normally distributed with mean $\boldsymbol{\mu} = \mathbb{E}\{\mathbf{y}_n - \mathbf{X}_n\mathbf{h}_n\} = \mathbf{0}$ and covariance matrix $\boldsymbol{\Sigma} = \mathbb{E}\{(\mathbf{y}_n - \mathbf{X}_n\mathbf{h}_n)(\mathbf{y}_n - \mathbf{X}_n\mathbf{h}_n)^H\} = \sigma^2_{\text{rad}}\mathbf{I}$, where $\sigma^2_{\text{rad}}$ denotes the noise variance. Subsequently, the log-likelihood function of RX frequency-domain symbols for all subcarriers, $\mathbf{y} = [\mathbf{y}^T_1, \ldots, \mathbf{y}^T_N]^T$, can then be written as

$$\log \mathcal{P}_{\mathbf{y}}(\mathbf{y}; \boldsymbol{\alpha}) = -\log\left(\sigma^2_{\text{rad}}\pi^{NML^{\text{RF}}_{\text{RX,rad}}}\right) - \frac{1}{\sigma^2_{\text{rad}}}\Bigg(\sum_{n=1}^{N} \mathbf{y}^H_n\mathbf{y}_n + \mathbf{h}^H_n\mathbf{X}^H_n\mathbf{X}_n\mathbf{h}_n - 2\Re\{\mathbf{y}^H_n\mathbf{X}_n\mathbf{h}_n\}\Bigg). \tag{42}$$

Each element of $\mathcal{I}(\boldsymbol{\alpha})$ can then be calculated as [4]

$$\mathcal{I}(\boldsymbol{\alpha})_{i,j} = -\mathbb{E}\left\{\frac{\partial^2 \log \mathcal{P}_{\mathbf{y}}(\mathbf{y}; \boldsymbol{\alpha})}{\partial\alpha_i \partial\alpha_j}\right\}, \tag{43}$$

where $i$ and $j$ are the row and column numbers. Next, twice differentiating (42) and simplifying results in an expression for (43) as

$$\mathcal{I}(\boldsymbol{\alpha})_{i,j} = \frac{2}{\sigma^2_{\text{rad}}}\Re\left\{\sum_{n=1}^{N} \frac{\partial \mathbf{h}^H_n}{\partial\alpha_j}\mathbf{P}_n\frac{\partial \mathbf{h}_n}{\partial\alpha_i}\right\}, \tag{44}$$

where the expectation between frequency-domain symbols, either on different streams or OFDM symbols, for the same subcarrier, is assumed to be zero. Then, $\mathbf{P}_n = \text{diag}\left\{|x_{n,1,1}|^2\mathbf{I}, \cdots, |x_{n,m,s}|^2\mathbf{I}, \cdots, |x_{n,M,S}|^2\mathbf{I}\right\}$.

To find each element of $\mathcal{I}(\boldsymbol{\alpha})$, partial derivatives of $\mathbf{h}_n$ are needed w.r.t. the DoA and delay estimates. These are then found using (11) as,

$$\frac{\partial \mathbf{h}_{n,m,s}}{\partial\tau} = (-\jmath 2\pi n\Delta f)be^{-\jmath 2\pi n\Delta f\tau}e^{\jmath 2\pi m\frac{f_{\text{D}}}{\Delta f}}\mathbf{g}_{n,m,s}, \tag{45}$$

where

$$\mathbf{g}_{n,m,s} = (\mathbf{W}^{\text{RF}}_{\text{RX,rad},m})^H\mathbf{a}_{\text{RX}}(\theta)\mathbf{a}^H_{\text{TX}}(\theta)\mathbf{W}^{\text{RF}}_{\text{TX},m}(\mathbf{W}^{\text{BB}}_{\text{TX},n,m})_s, \tag{46}$$

and thus

$$\frac{\partial \mathbf{h}_{n,m}}{\partial\tau} = (-\jmath 2\pi n\Delta f)be^{-\jmath 2\pi n\Delta f\tau}e^{\jmath 2\pi m\frac{f_{\text{D}}}{\Delta f}}\mathbf{g}_{n,m}, \tag{47}$$

where $\mathbf{g}_{n,m} = [\mathbf{g}^T_{n,m,1}, \cdots, \mathbf{g}^T_{n,m,S}]^T$. Next, using (8),

$$\frac{\partial \mathbf{a}(\theta)}{\partial\theta} = \left[0, \ldots, e^{\jmath\pi(L-1)\sin(\theta)}\jmath\pi(L-1)\cos(\theta)\right]^T = \jmath\pi\cos(\theta)\mathbf{D}\mathbf{a}(\theta), \tag{48}$$

where $\mathbf{D} = \text{diag}\{[0, \ldots, L-1]\}$ denotes a diagonal matrix, and therefore

$$\frac{\partial \mathbf{h}_{n,m,s}}{\partial\theta} = \jmath\pi be^{-\jmath 2\pi n\Delta f\tau}e^{\jmath 2\pi m\frac{f_{\text{D}}}{\Delta f}}\cos(\theta)\mathbf{g}'_{n,m,s}, \tag{49}$$

where

$$\mathbf{g}'_{n,m,s} = (\mathbf{W}^{\text{RF}}_{\text{RX,rad},m})^H \Big( \mathbf{D}_{\text{RX}} \mathbf{a}_{\text{RX}}(\theta) \mathbf{a}^H_{\text{TX}}(\theta) - \mathbf{a}_{\text{RX}}(\theta) \mathbf{a}^H_{\text{TX}}(\theta) \mathbf{D}_{\text{TX}} \Big) \mathbf{W}^{\text{RF}}_{\text{TX},m} (\mathbf{W}^{\text{BB}}_{\text{TX},n,m})_s. \quad (50)$$

Thus,

$$\frac{\partial \mathbf{h}_{n,m}}{\partial \theta} = \jmath \pi b e^{-\jmath 2\pi n \Delta f \tau_k} e^{\jmath 2\pi m \frac{f_{\text{D}}}{\Delta f}} \cos(\theta) \mathbf{g}'_{n,m}, \quad (51)$$

where $\mathbf{g}'_{n,m} = [(\mathbf{g}'_{n,m,1})^T, \cdots, (\mathbf{g}'_{n,m,S})^T]^T$. Next, based on (44), individual elements of $\mathcal{I}(\boldsymbol{\alpha})$ can be derived as

$$\mathcal{I}(\boldsymbol{\alpha})_{1,1} = 2\pi^2 \cos^2(\theta)(\text{SNR}) \cdot \sum_{m=1}^{M} \sum_{n=1}^{N} \sum_{s=1}^{S} P_{n,m,s} (\mathbf{g}'_{n,m,s})^H \mathbf{g}'_{n,m,s}, \quad (52)$$

$$\mathcal{I}(\boldsymbol{\alpha})_{2,2} = 8\pi^2 (\Delta f)^2 (\text{SNR}) \cdot \sum_{m=1}^{M} \sum_{n=1}^{N} \sum_{s=1}^{S} \bar{n}^2 P_{n,m,s} (\mathbf{g}_{n,m,s})^H \mathbf{g}_{n,m,s}, \quad (53)$$

$$\mathcal{I}(\boldsymbol{\alpha})_{1,2} = -4\pi^2 (\Delta f) \cos(\theta)(\text{SNR}) \cdot \Re \left\{ \sum_{m=1}^{M} \sum_{n=1}^{N} \sum_{s=1}^{S} \bar{n} P_{n,m,s} (\mathbf{g}_{n,m,s})^H \mathbf{g}'_{n,m,s} \right\}, \quad (54)$$

where $P_{n,m,s} = \frac{|x_{n,m,s}|^2}{P_{\text{t}}}$, $\text{SNR} = \frac{P_{\text{t}}}{\sigma^2_{\text{rad}}}$, while $\mathcal{I}(\boldsymbol{\alpha})_{2,1} = \mathcal{I}(\boldsymbol{\alpha})_{1,2}$. Then, CRLBs of delay and DoA estimates are given by the diagonal elements of $\mathcal{I}^{-1}(\boldsymbol{\alpha})$ as [43]

$$\text{CRLB}(\hat{\theta}) = \frac{1}{2\pi^2 \cos^2(\theta)(\text{SNR}) f_\theta(\mathbf{P})}, \quad (55)$$

$$\text{CRLB}(\hat{\tau}) = \frac{1}{8\pi^2 (\Delta f)^2 (\text{SNR}) f_\tau(\mathbf{P})}, \quad (56)$$

where

$$f_\theta(\mathbf{P}) = \sum_{m=1}^{M} \sum_{n=1}^{N} \sum_{s=1}^{S} P_{n,m,s} (\mathbf{g}'_{n,m,s})^H \mathbf{g}'_{n,m,s} - \frac{\left( \Re \left\{ \sum_{m=1}^{M} \sum_{n=1}^{N} \sum_{s=1}^{S} \bar{n} P_{n,m,s} (\mathbf{g}_{n,m,s})^H \mathbf{g}'_{n,m,s} \right\} \right)^2}{\sum_{m=1}^{M} \sum_{n=1}^{N} \sum_{s=1}^{S} \bar{n}^2 P_{n,m,s} (\mathbf{g}_{n,m,s})^H \mathbf{g}_{n,m,s}}, \quad (57a)$$

$$f_\tau(\mathbf{P}) = \sum_{m=1}^{M} \sum_{n=1}^{N} \sum_{s=1}^{S} \bar{n}^2 P_{n,m,s} (\mathbf{g}_{n,m,s})^H \mathbf{g}_{n,m,s} - \frac{\left( \Re \left\{ \sum_{m=1}^{M} \sum_{n=1}^{N} \sum_{s=1}^{S} \bar{n} P_{n,m,s} (\mathbf{g}_{n,m,s})^H \mathbf{g}'_{n,m,s} \right\} \right)^2}{\sum_{m=1}^{M} \sum_{n=1}^{N} \sum_{s=1}^{S} P_{n,m,s} (\mathbf{g}'_{n,m,s})^H \mathbf{g}'_{n,m,s}}. \quad (57b)$$

Moreover, $\mathbf{P}$ is the matrix of power of the subcarriers of the communications and sensing streams.

### *B. Joint CRLB Minimization*

**Optimization problem 1.** ***(Joint optimization)*** *Subcarriers of the sensing streams are optimized to minimize the CRLBs of DoA and delay estimates jointly through the optimization problem given as*

$$\min_{\boldsymbol{x}_{rad,n,m}, \mathcal{R}_{n,m,\tilde{s}}} \text{CRLB}(\hat{\theta}) \quad (58a)$$

*subject to*

$$\text{CRLB}(\hat{\tau}) \leq \tau^2_{\max}, \quad (58b)$$

$$\frac{\zeta_{\text{int,com}}}{\bar{\zeta}_{\text{com}}} = \eta, \quad (58c)$$

$$P_{\text{rad}} \leq P_{\text{t}} - P_{\text{com}}, \quad (58d)$$

$$0 \leq P_{n,m,\tilde{s}} \leq P_{\max}, \tilde{s} \in [1, U_{\text{rad}}]. \quad (58e)$$

The goal of the optimization is thus to find the frequency-domain symbols of the radar streams $\mathbf{x}_{\text{rad},n,m}$, together with the set of indices of the activated subcarriers in sensing streams $\mathcal{R}_{n,m,\tilde{s}}$. In addition, the power of a subcarrier in a sensing stream is limited by (58e). The equality constraint (58c) ensures some specific sum communication capacity of the JCAS system when compared to that of when only communication is performed, i.e., without JCAS, as derived in (22) and (23). Here, $\eta \in [0, 1]$, and when beamforming design is fixed, varying $P_{\text{com}}$ implies varying $\eta$, and thus, $\eta = f(P_{\text{com}})$, where $f(\cdot)$ is some function. Hence, conversely, choosing a specific $\eta$ value defines $P_{\text{com}}$.

Due to the vast search space, the solution to the optimization cannot be found straightforwardly, and hence a two-fold approach is used. First, assuming the optimally activated subcarrier indices of the sensing streams are known, the minimum $\text{CRLB}(\hat{\theta})$ is given by the following theorem.

**Theorem 1.** *In solving the joint optimization problem, $N_{\text{act}} - 1$ subcarriers of the radar streams receive a power of $P_{\max}$ while a single subcarrier with indices $\{n_0, m_0, \tilde{s}_0\}$ receives a power of $P_\Delta$. In this case, minimum $\text{CRLB}(\hat{\theta})$ is given by (59). Here,*

$$\bar{n} = n - \frac{N+1}{2}, \quad (60)$$

$$\text{DEN}_{\text{com}} = \sum_{m=1}^{M} \sum_{n=1}^{N} \sum_{s=1}^{S_{\text{com}}} P_{n,m,s} (\boldsymbol{g}'_{n,m,s})^H \boldsymbol{g}'_{n,m,s}, \quad (61)$$

$$\text{NUM}_{\text{com}} = \sum_{m=1}^{M} \sum_{n=1}^{N} \sum_{s=1}^{S_{\text{com}}} \bar{n}^2 P_{n,m,s} (\boldsymbol{g}_{n,m,s})^H \boldsymbol{g}_{n,m,s}, \quad (62)$$

$$N_{\text{act}} = \left\lceil \frac{P_{\text{t}} - P_{\text{com}}}{P_{\max}} \right\rceil, \quad (63)$$

$$P_\Delta = P_{\text{t}} - P_{\text{com}} - P_{\max}(N_{\text{act}} - 1). \quad (64)$$

*Here, $\lceil . \rceil$ represents the ceiling operation, $N_{\text{act}}$ is the number of subcarriers of all $U_{\text{rad}}$ radar streams that are activated, while $\boldsymbol{g}_{n,m,\tilde{s}}$ and $\boldsymbol{g}'_{n,m,\tilde{s}}$ are based on (46) and (50).*

*Proof.* See Appendix A. □

The next step is identifying the optimum subcarrier indices that minimize the expression in (59). For this, the denominator should be maximized while simultaneously minimizing the numerator. Interestingly, the denominator and numerator in (59) correspond to $\mathcal{I}(\boldsymbol{\alpha})_{1,1}$ from (52) and $\mathcal{I}(\boldsymbol{\alpha})_{2,2}$ from (53), respectively, which in turn which correspond to $\mathcal{I}(\boldsymbol{\alpha})$ values when only one parameter needs to be estimated, i.e., denominator $\theta$–only, and numerator $\tau$–only. Therefore, these separate minimization problems are used to determine the optimum joint optimization indices.

$$\text{CRLB}(\hat{\theta}) = \tau_{\text{max}}^2 \frac{4(\Delta f)^2}{\cos^2(\theta)} \cdot \frac{\text{NUM}_{\text{com}} + P_{\text{max}} \sum_{m=1}^{M} \sum_{\tilde{s}=1}^{U_{\text{rad}}} \sum_{n \in \mathcal{R}_{n,m,\tilde{s}}} \bar{n}^2 (\mathbf{g}_{n,m,\tilde{s}})^H \mathbf{g}_{n,m,\tilde{s}} + P_{\Delta} \bar{n}_0^2 (\mathbf{g}_{n_0,m_0,\tilde{s}_0})^H \mathbf{g}_{n_0,m_0,\tilde{s}_0}}{\text{DEN}_{\text{com}} + P_{\text{max}} \sum_{m=1}^{M} \sum_{\tilde{s}=1}^{U_{\text{rad}}} \sum_{n \in \mathcal{R}_{n,m,\tilde{s}}} (\mathbf{g}'_{n,m,\tilde{s}})^H \mathbf{g}'_{n,m,\tilde{s}} + P_{\Delta} (\mathbf{g}'_{n_0,m_0,\tilde{s}_0})^H \mathbf{g}'_{n_0,m_0,\tilde{s}_0}} \tag{59}$$

$$\text{CRLB}(\hat{\theta})_{\text{sep}} = \frac{1}{2\pi^2 \cos^2(\theta)(\text{SNR})} \cdot \frac{1}{\text{DEN}_{\text{com}} + P_{\text{max}} \sum_{m=1}^{M} \sum_{\tilde{s}=1}^{U_{\text{rad}}} \sum_{n \in \mathcal{R}_{n,m,\tilde{s}}} (\mathbf{g}'_{n,m,\tilde{s}})^H \mathbf{g}'_{n,m,\tilde{s}} + P_{\Delta} (\mathbf{g}'_{n_0,m_0,\tilde{s}_0})^H \mathbf{g}'_{n_0,m_0,\tilde{s}_0}} \tag{65}$$

$$\text{CRLB}(\hat{\tau})_{\text{sep}} = \frac{1}{8\pi^2 (\Delta f)^2 (\text{SNR})} \cdot \frac{1}{\text{NUM}_{\text{com}} + P_{\text{max}} \sum_{m=1}^{M} \sum_{\tilde{s}=1}^{U_{\text{rad}}} \sum_{n \in \mathcal{R}_{n,m,\tilde{s}}} \bar{n}^2 (\mathbf{g}_{n,m,\tilde{s}})^H \mathbf{g}_{n,m,\tilde{s}} + P_{\Delta} \bar{n}_0^2 (\mathbf{g}_{n_0,m_0,\tilde{s}_0})^H \mathbf{g}_{n_0,m_0,\tilde{s}_0}} \tag{66}$$

TABLE II
CRLB OPTIMIZATION PARAMETERS

| Parameter | Definition |
|---|---|
| $\text{CRLB}(\hat{\theta})$ | CRLB of the DoA estimate |
| $\text{CRLB}(\hat{\tau})$ | CRLB of the delay estimate |
| $\tau_{\text{max}}^2$ | Maximum CRLB delay value |
| $P_{\text{rad}}$ | Power for the sensing streams |
| $P_{\text{com}}$ | Power for the communications streams |
| $P_{\text{t}}$ | All streams' total power |
| $P_{n,m,\tilde{s}}$ | Subcarrier power of a sensing stream |
| $P_{\text{max}}$ | Maximum power of a sensing subcarrier |
| $P_{\Delta}$ | Residual power to one sensing subcarrier |
| $N_{\text{act}}$ | Number of activated sensing subcarriers |

**Optimization problem 2.** ***(Separate minimization)***
**(a)** $\min_{\boldsymbol{x}_{rad,n,m}, \mathcal{R}_{n,m,\tilde{s}}} \text{CRLB}(\hat{\theta})$ *subject to* $\frac{\zeta_{\text{int,com}}}{\zeta_{\text{com}}} = \eta$, $P_{\text{rad}} \leq P_{\text{t}} - P_{\text{com}}$, *and* $0 \leq P_{n,m,\tilde{s}} \leq P_{\text{max}}, \tilde{s} \in [1, U_{\text{rad}}]$,
**(b)** $\min_{\boldsymbol{x}_{rad,n,m}, \mathcal{R}_{n,m,\tilde{s}}} \text{CRLB}(\hat{\tau})$ *subject to* $\frac{\zeta_{\text{int,com}}}{\zeta_{\text{com}}} = \eta$, $P_{\text{rad}} \leq P_{\text{t}} - P_{\text{com}}$, *and* $0 \leq P_{n,m,\tilde{s}} \leq P_{\text{max}}, \tilde{s} \in [1, U_{\text{rad}}]$.

The following theorem gives the optimal subcarrier indices of the sensing streams for the two separate optimizations.

**Theorem 2.** *For (a) minimum* $\text{CRLB}(\hat{\theta})$*, subcarriers of the sensing streams having maximized* $(\mathbf{g}'_{n,m,\tilde{s}})^H \mathbf{g}'_{n,m,\tilde{s}}$ *are activated, while for (b) minimum* $\text{CRLB}(\hat{\tau})$*, subcarriers of the sensing streams having maximized* $\bar{n}^2 (\mathbf{g}_{n,m,\tilde{s}})^H \mathbf{g}_{n,m,\tilde{s}}$ *are activated.*

*Proof.* For (a) the separate minimization of $\text{CRLB}(\hat{\theta})$, (52) is the only element of $\mathcal{I}(\boldsymbol{\alpha})$, and the corresponding CRLB value is given by (65). Here, SNR denotes the signal-to-noise ratio (SNR) at the MIMO RX. To minimize (65), the denominator needs to be maximized, and thus, the subcarriers of sensing streams should be activated sequentially according to the product $(\mathbf{g}'_{n,m,\tilde{s}})^H \mathbf{g}'_{n,m,\tilde{s}}$. Similarly, for (b) the separate minimization of $\text{CRLB}(\hat{\tau})$, the single element of $\mathcal{I}(\boldsymbol{\alpha})$ is given by (53), and hence the corresponding CRLB value is given by (66). Here, subcarriers of the sensing streams should be chosen so as to maximize the term $\bar{n}^2 (\mathbf{g}_{n,m,\tilde{s}})^H \mathbf{g}_{n,m,\tilde{s}}$. □

These separate minimization problems are then used to arrive at the subcarriers of the sensing streams that are activated in the joint optimization by the following theorem.

**Theorem 3.** *The activated subcarrier indices of the sensing streams can be calculated based on Algorithm 2.*

*Proof.* The algorithm starts with the waveform having the minimum $\text{CRLB}(\hat{\theta})$, according to (65). Hence, $N_{\text{act}}$ subcarriers of the sensing streams having the highest $(\mathbf{g}'_{n,m,\tilde{s}})^H \mathbf{g}'_{n,m,\tilde{s}}$ are activated. Then, the frequency-domain symbols of the activated subcarriers having the least $(\mathbf{g}'_{n,m,\tilde{s}})^H \mathbf{g}'_{n,m,\tilde{s}}$ are moved sequentially to unactivated subcarriers having the highest $\bar{n}^2 (\mathbf{g}_{n,m,\tilde{s}})^H \mathbf{g}_{n,m,\tilde{s}}$. Doing so for $N_{\text{act}}$ activated subcarriers results in the waveform with the minimum $\text{CRLB}(\hat{\tau})$.

□

The activated subcarrier indices are critical in solving Optimization problem 1. For this, the products $(\mathbf{g}'_{n,m,\tilde{s}})^H \mathbf{g}'_{n,m,\tilde{s}}$ and $\bar{n}^2 (\mathbf{g}_{n,m,\tilde{s}})^H \mathbf{g}_{n,m,\tilde{s}}$ are necessary to be calculated. Thus, TX and RX beamforming matrices, $N$ and $M$, mainly contribute to the computational complexity of waveform optimization. Generally, $N$ is the main bottleneck since it is quite high but simultaneously increases the range resolution of the radar system, indicating its trade-off.

Finally, the CRLB optimization in (58a)–(58e) only optimizes $\mathbf{x}_{\text{rad},n,m}$ and $\mathcal{R}_{n,m,\tilde{s}}$, assuming that $\mathbf{W}_{\text{TX,rad},n,m}^{\text{BB}}$ is given. However, a better solution can be obtained by also optimizing $\mathbf{W}_{\text{TX,rad},n,m}^{\text{BB}}$. Since we design it based on (39) to cancel radar–communications interference, that flexibility is not there. If necessary, $\mathbf{W}_{\text{TX,rad},n,m}^{\text{BB}}$ can also be optimized for better CRLBs, but at the cost of increasing the interference.

## V. NUMERICAL RESULTS

Here we analyze the performance of the proposed beamforming, waveform optimization, and radar processing. For the simulations, the following parameters are used: $f_{\text{com}} = 28$ GHz, $L_{\text{TX}} = L_{\text{RX,rad}} = 32$, $L_{\text{TX}}^{\text{RF}} = L_{\text{RX,rad}}^{\text{RF}} = 8$, $U_{\text{com}} = 2$, $S_{\text{com},u} = 2$, $S_{\text{com}} = 4$, $U_{\text{rad}} = 2$, $M = 50$, $P_{\text{t}} = 40$ dBm and SNR $= 10$ dB. Further, we use $N = 3168$ with $\Delta f = 120$ kHz, as specified in the 5G standards [39]. The power allocated to the communication streams is chosen for a specific

**Algorithm 2** Calculation of sensing streams' optimal subcarrier indices for joint minimization

Set $z = 0$
Set $\mathcal{R}$ as set of subcarrier indices for sensing streams
Set $\hat{\mathcal{R}}$ as sensing streams' activated subcarriers having the highest $(\mathbf{g}'_{n,m,\tilde{s}})^H \mathbf{g}'_{n,m,\tilde{s}}$, in descending order
**while** $z \leq N_{\text{act}}$ **do**
    Calculate CRLB$(\hat{\theta})_z$ and CRLB$(\hat{\tau})_z$
    Set $\mathcal{R}' = (\mathcal{R} \cap \hat{\mathcal{R}})'$
    Move the symbol of activated subcarrier in $\hat{\mathcal{R}}$ with the least $(\mathbf{g}'_{n,m,\tilde{s}})^H \mathbf{g}'_{n,m,\tilde{s}}$ to the unactivated subcarrier in $\mathcal{R}'$ with the highest $\bar{n}^2 (\mathbf{g}_{n,m,\tilde{s}})^H \mathbf{g}_{n,m,\tilde{s}}$
    Update the set $\hat{\mathcal{R}}$
    $z \leftarrow z + 1$

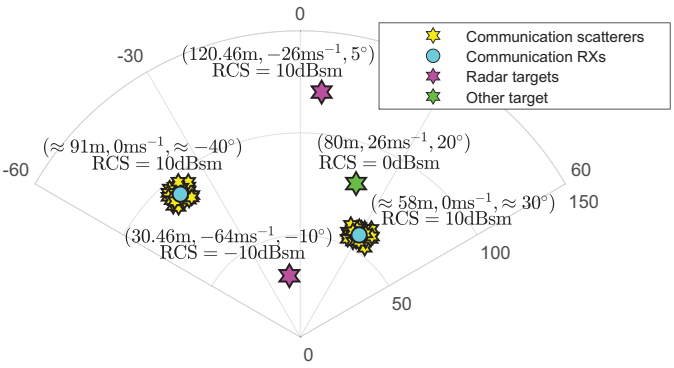


Fig. 2. Considered scenario for the simulations with five sets of targets having the given ranges, velocities, angles and RCSs.

$\eta$ value as $P_{\text{com}} = f^{-1}(\eta)$, since $\eta = f(P_{\text{com}}) = f(\beta P_{\text{t}})$, where $\beta \in [0, 1]$, and it controls the power allocation between communications and sensing streams. All beamforming matrices remain the same for a set of OFDM symbols, which is a valid assumption in mm-wave channels since it is difficult for the MIMO TRX to acquire information about the fast-changing channel per OFDM symbol.

Firstly, Fig. 2 illustrates the scenario for simulations. The two communications user directions are given by $\boldsymbol{\theta}_{\text{com}} = \{-40°, 30°\}$. Additionally, to simulate the NLoS multipath communications channel, 20 point targets act as scatterers distributed randomly in a cloud surrounding the corresponding communications RX. The MIMO channel is obtained based on the delay, Doppler-shift, and angle of the scatterers w.r.t. the MIMO TX, using (14). There are two point targets at the sensing directions given by $\boldsymbol{\theta}_{\text{rad}} = \{-10°, 5°\}$, to which radar streams are transmitted. Moreover, there is an ´other' target at 20°, different from communications and sensing directions. The radar cross-sections (RCSs) of different targets are also illustrated in the figure. Moreover, all targets are considered to have frequency-flat responses.

Figure 3 then depicts the total TX beampatterns, i.e., the combination of both RF and baseband beamforming. Additionally, they are the average of different TX streams. Here, $\rho$ is as defined in (33). For the sensing-only case, gains at sensing directions are maximized while those at the communication directions are attenuated ca. 20 dB. Then, for the communications-only case, the beampattern is no longer directional, due to communication users being in NLoS conditions and it is designed to cancel inter-user and intra-user interference. Moreover, gains at the sensing directions are attenuated ca. 20 dB from the sensing-only case. Finally, for the JCAS case, gains at both communications and sensing directions are almost similar, showing that all streams are transmitted to both sets of directions.

Next, the effect of $\eta$ in (58c) on $\beta$, i.e., $P_{\text{com}}$ (since $P_{\text{com}} = \beta P_{\text{t}}$), is shown in Fig. 4, also for different $\rho$ values. For a specific $\rho$ value, an increase of $\eta$ also implies an increase of $\beta$ to increase communication performance. Depending on the required $\eta$, less $P_{\text{com}}$ is required if $\rho$ can be increased since it increases the gains for communications. However, as discussed later, sensing performance decreases with the increase of these

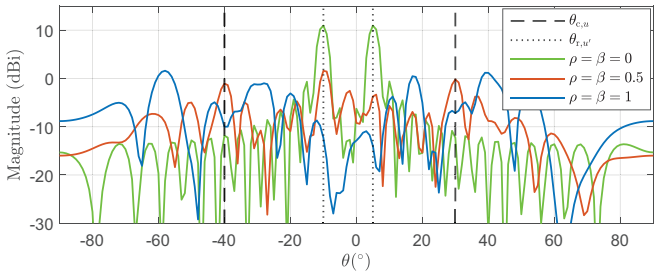


Fig. 3. TX beampatterns for three scenarios: $\rho, \beta = 0$ (sensing-only), $\rho, \beta = 0.5$ (JCAS), and $\rho, \beta = 1$ (communications-only), for a single subcarrier.

parameters. Hence, it is important to select these parameters depending on the required level of performance for the two functionalities.

Next, sensing streams are optimized as in Optimization problem 1, shown in Fig. 5. First, Fig. 5(a) illustrates root CRLBs as a function of SNR for separate optimization problems defined in Optimization problem 2. For the DoA estimate, $\theta = 5°$. Here, $P_{\text{max}}$ is chosen so that the power ratio between it and the power of a subcarrier in a communications stream is four, i.e., $10\log(P_{\text{max}}) - 10\log(\frac{P_{\text{com}}}{MNS_{\text{com}}}) = 6$ dB. The figure also shows the CRLBs when it is 10 dB. When $\rho$ decreases, CRLBs decrease due to increased gains of TX RF beamforming. Increasing power difference also decreases CRLBs since it decreases the number of activated subcarriers for an increased $P_{\text{max}}$ value (63), allowing to maximize (57a) and (57b), thereby decreasing the CRLBs. Figure 5(b) illustrates the trade-off between the two CRLBs, for a fixed SNR of 10 dB. Here, decreasing $\beta$ decreases the CRLBs due to increased power for the sensing streams. It is observed that the absolute values of the root CRLBs vary slightly due to the optimization. However, optimizing the waveform minimizes the CRLBs compared to the unoptimized case.

The sensing performance is then evaluated through the empirical receiver operating characteristics (ROC) for the radar target at 5°, and it is shown in Fig. 6(a). The target's range is uniformly distributed over many iterations, keeping the angle fixed. Then, for each iteration, the average power value of the range–angle map is calculated for a rectangular area of sides 1.58m and 4°, centered around the target's supposed range and

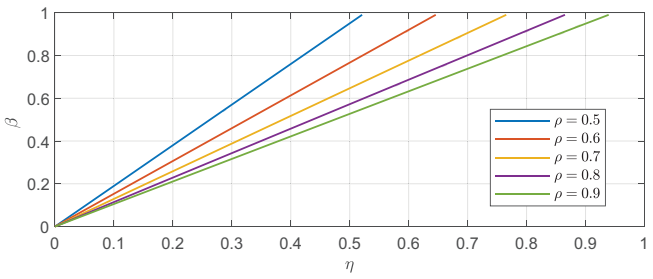


Fig. 4. Variation of $\beta$ for different $\eta$ values.

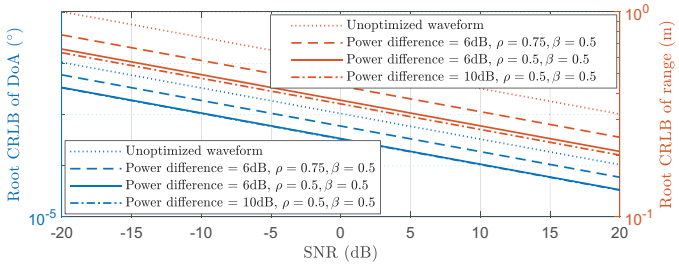


(a) Root CRLBs of DoA and range as a function of SNR

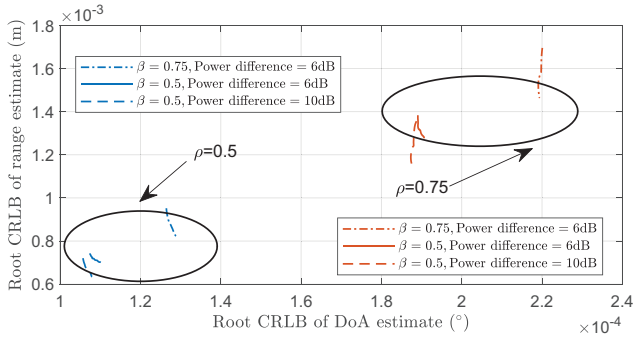


(b) Root CRLB trade-off, where the point corresponding to $\rho = \beta = 1$ (unoptimized waveform) is given by $(0.000332°, 0.032m)$

Fig. 5. Variation of the root CRLBs with different $\rho$, $\beta$, power difference and SNR values.

angle. The values obtained for the different iterations are then used to calculate the probabilities of detection and false alarm (without a target). Secondly, the root mean square errors (RMSEs) of the two estimates are calculated, as shown in Figs. 6(b) and (c). All three figures show sensing performance improves as either $\rho$ or $\beta$ decreases because more power is allocated for sensing. Thus, although the joint optimization minimizes the CRLBs slightly, it improves the sensing performance in a practical scenario.

Finally, Fig. 7 illustrates the range–angle and range–velocity maps. For the sensing-only case, $95\%$ of sensing streams' subcarriers are activated. Here, the two radar targets are clearly detected in the range–angle map. Their velocities are also clearly observed in the range–velocity map while observing the velocities of communication scatterers and the 'other' target. In addition, there is some spreading of the velocities of radar targets, which could most likely be due to the approximated steering vector in (8). Regardless, the targets' velocities can be reliably detected. However, (7) needs to be used instead of (8) for systems where the bandwidth w.r.t. the carrier

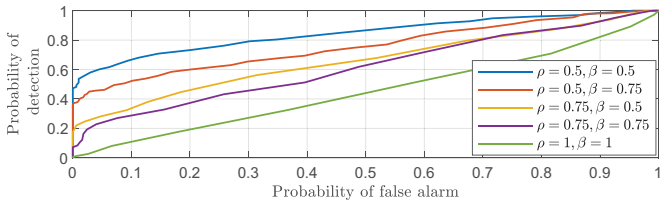


(a) ROC curve

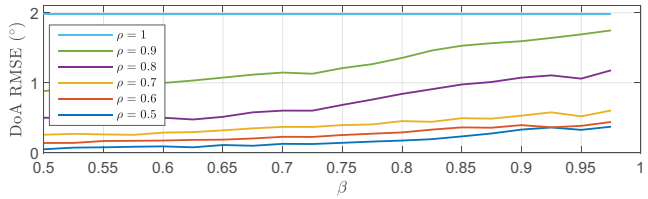


(b) DoA estimate

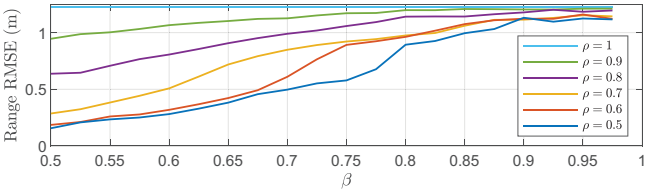


(c) Range estimate

Fig. 6. The sensing performance of the radar target at $5°$ evaluated through the ROC and RMSEs of DoA and range estimates.

frequency is high, to prevent degrading radar performance. For the communications-only case, however, the parameters are difficult to detect while not being consistent with the actual target parameters. For the JCAS case, all targets are clearly detected. Hence, the proposed radar processing illustrates that sharing some portion of the communication streams to the radar streams allows to obtain a better map of the environment.

Once either map is obtained, more information is required to differentiate between the communication scatterers and the radar targets. Since the communications streams are transmitted at the users, some beamforming is required, as illustrated in Fig. 3. This angular information could then be used in conjunction with the range–angle map to differentiate between the communication scatterers and radar targets in the angular domain and subsequently in the range domain. Next, the range information can be used to distinguish in the velocity domain using the range–velocity map. Moreover, in target tracking, communication scatterers may remain more likely static while radar targets inherently move between successive maps, based on the scenario depicted in Fig. 2. Hence, successive maps can be used for the differentiation, i.e., communication scatterers having slowly changing ranges and angles, while radar targets have varying ranges and angles.

## VI. Conclusion

This study concerned radar processing for a MIMO-OFDM communications system with hybrid architecture, performing JCAS. The MIMO TX caters to multiple users with multiple streams over frequency-selective NLoS channels. Sens-

ing streams are transmitted concurrently in sensing directions, different from communications. Additionally, optimized frequency-domain samples are used for sensing streams that jointly minimize CRLBs of range and DoA estimates. Simulations illustrate that communications and sensing targets can be reliably detected through MIMO processing. The ROC and RMSEs of DoA and range estimates can be improved by allocating more power for sensing, indicating the effectiveness of the waveform optimization. Moreover, the optimization parameters need to be selected based on the application to obtain the required level of trade-off between the communications capacity and the sensing performance.

## APPENDIX A
## SOLUTION TO THE OPTIMIZATION PROBLEM

Differentiating (55) w.r.t. the power of a subcarrier in a sensing stream $P_{n,m,\tilde{s}}$, with $\tilde{s} \in [1, U_{\text{rad}}]$, and simplifying gives

$$\frac{\partial \text{CRLB}(\hat{\theta})}{\partial P_{n,m,\tilde{s}}} = \left(\frac{-1}{2\pi^2 \cos^2(\theta)(\text{SNR})}\right)\left(\frac{|g_{n,m,s}|^2}{f_\theta^2(\mathbf{P})}\right)\left|\frac{g'_{n,m,\tilde{s}}}{g_{n,m,s}} - \frac{\bar{n}\left(\Re\left\{\sum_{m=1}^{M}\sum_{n=1}^{N}\sum_{s=1}^{S}\bar{n}P_{n,m,s}(\mathbf{g}_{n,m,s})^H\mathbf{g}'_{n,m,s}\right\}\right)}{\left(\sum_{m=1}^{M}\sum_{n=1}^{N}\sum_{s=1}^{S}\bar{n}^2 P_{n,m,s}(\mathbf{g}_{n,m,s})^H\mathbf{g}_{n,m,s}\right)}\right|^2. \tag{67}$$

For a given $\{n, m, \tilde{s}\}$ pair, $\frac{\partial \text{CRLB}(\hat{\theta})}{\partial P_{n,m,\tilde{s}}} \neq 0$ due to the needed relation between $g'_{n,m,\tilde{s}}$ and $g_{n,m,\tilde{s}}$. As such, $\frac{\partial \text{CRLB}(\hat{\theta})}{\partial P_{n,m,\tilde{s}}} < 0$, meaning that $\text{CRLB}(\hat{\theta})$ always decreases when $P_{n,m,\tilde{s}}$ increases. Thus, the constraint (58d) simplifies into equality. Next, using (55)–(57b), relation between the two CRLBs is as $\frac{\text{CRLB}(\hat{\theta})}{\text{CRLB}(\hat{\tau})} = \frac{4(\Delta f)^2}{\cos^2(\theta)} \frac{\sum_{m=1}^{M}\sum_{n=1}^{N}\sum_{s=1}^{S}\bar{n}^2 P_{n,m,s}(\mathbf{g}_{n,m,s})^H\mathbf{g}_{n,m,s}}{\sum_{m=1}^{M}\sum_{n=1}^{N}\sum_{s=1}^{S} P_{n,m,s}(\mathbf{g}'_{n,m,s})^H\mathbf{g}'_{n,m,s}}$, and thus as $\text{CRLB}(\hat{\theta}) = \text{CRLB}(\hat{\tau}) f(\mathbf{P})$. Then, using (58b),

$$\text{CRLB}(\hat{\theta}) \leq \tau_{\max}^2 f(\mathbf{P}), \tag{68}$$

and this is used instead of (58b). The derivative of $f(\mathbf{P})$ is given by (69), and its sign can be evaluated based on $\frac{\partial f(\mathbf{P})}{\partial P_{n,m,\tilde{s}}} \gtrless 0$, which after some simplification steps, can be written as in (70). It can then be assumed that $\gamma_1 \ll 1$, while $\gamma_2 \ggg 1$ because $\gamma_2$ has $\bar{n}^2$ term, which increases the value quite fast. Hence, $\gamma_1\gamma_2 > 1$, and thus $\frac{\partial f(\mathbf{P})}{\partial P_{n,m,\tilde{s}}} < 0, \forall n, m, \tilde{s}$.

The Lagrangian is then used, as given in (71), where $\lambda_1$, $\boldsymbol{\lambda}_2$, $\boldsymbol{\lambda}_3$, and $\lambda_4$ correspond to the Karush–Kuhn–Tucker (KKT) multipliers of the total power of the sensing streams, lower and upper bounds of the power constraint for a subcarrier in a sensing stream, and the inequality constraint in (68). Next, the following KKT conditions need to be satisfied for optimality:

$$\frac{\partial \mathcal{L}(\mathbf{P}, \lambda_1, \boldsymbol{\lambda}_2, \boldsymbol{\lambda}_3, \lambda_4)}{\partial P_{n,m,\tilde{s}}} = \frac{\partial \text{CRLB}(\hat{\theta})}{\partial P_{n,m,\tilde{s}}}(1-\lambda_4) - \lambda_1 - \lambda_{2,n,m,\tilde{s}} - \lambda_{3,n,m,\tilde{s}} + \lambda_4\tau_{\max}^2\frac{\partial f(\mathbf{P})}{\partial P_{n,m,\tilde{s}}} = 0, \tag{72}$$

$$\sum_{m=1}^{M}\sum_{n=1}^{N}\sum_{\tilde{s}=1}^{U_{\text{rad}}} P_{n,m,\tilde{s}} = P_{\text{t}} - P_{\text{com}}, \tag{73}$$

$$\lambda_{2,n,m,\tilde{s}} P_{n,m,\tilde{s}} = 0, \tag{74}$$

$$\lambda_{3,n,m,\tilde{s}}(P_{\max} - P_{n,m,\tilde{s}}) = 0, \tag{75}$$

$$\lambda_4\left(\tau_{\max}^2 f(\mathbf{P}) - \text{CRLB}(\hat{\theta})\right) = 0, \tag{76}$$

$$\lambda_{2,n,m,\tilde{s}} \geq 0, \tag{77}$$

$$\lambda_{3,n,m,\tilde{s}} \geq 0, \tag{78}$$

$$\lambda_4 \geq 0, \tag{79}$$

$$P_{n,m,\tilde{s}} \leq P_{\max}, \tag{80}$$

$$P_{n,m,\tilde{s}} \geq 0, \tag{81}$$

$$\text{CRLB}(\hat{\theta}) \leq \tau_{\max}^2 f(\mathbf{P}). \tag{82}$$

Since (72) needs to be satisfied for all $\{n, m, \tilde{s}\}$ pairs, either $\lambda_{2,n,m,\tilde{s}} \neq 0$ or $\lambda_{3,n,m,\tilde{s}} \neq 0$. Hence, based on (74) and (75), this means that $N_{\text{act}}$ subcarriers are activated with $P_{\max}$ power.

To satisfy (68), KKT conditions are (76), (79) and (82). If $\lambda_4 = 0$, (72) can be rewritten as

$$\frac{\partial \mathcal{L}(\mathbf{P}, \lambda_1, \boldsymbol{\lambda}_2, \boldsymbol{\lambda}_3)}{\partial P_{n,m,\tilde{s}}} = \frac{\partial \text{CRLB}(\hat{\theta})}{\partial P_{n,m,\tilde{s}}} - \lambda_{2,n,m,\tilde{s}} - \lambda_{3,n,m,\tilde{s}} - \lambda_1, \tag{83}$$

where sum of first three terms is negative since $\frac{\partial \text{CRLB}(\hat{\theta})}{\partial P_{n,m,\tilde{s}}} < 0$ from (67) and $\lambda_{2,n,m,\tilde{s}}, \lambda_{3,n,m,\tilde{s}} > 0$. Then, for (83) to be zero, a value can be found for $\lambda_1$, but only for one $\{n, m, \tilde{s}\}$ pair, and not for all. Therefore, $\lambda_4 \neq 0$, and from (76), $\text{CRLB}(\hat{\theta}) = \tau_{\max}^2 f(\mathbf{P})$, making (58b) an equality. In this case, $\frac{\partial \text{CRLB}(\hat{\theta})}{\partial P_{n,m,\tilde{s}}}(1-\lambda_4) + \lambda_4\tau_{\max}^2\frac{\partial f(\mathbf{P})}{\partial P_{n,m,\tilde{s}}} - \lambda_1 > 0$, in (72), and after some simplifying, $\lambda_4 < 1 - \frac{\tau_{\max}^2\left|\frac{\partial f(\mathbf{P})}{\partial P_{n,m,\tilde{s}}}\right| + \lambda_1}{\tau_{\max}^2\left|\frac{\partial f(\mathbf{P})}{\partial P_{n,m,\tilde{s}}}\right| - \left|\frac{\partial \text{CRLB}(\hat{\theta})}{\partial P_{n,m,\tilde{s}}}\right|}$. Then, choosing $\lambda_1 < 0$ and $|\lambda_1| > \left|\frac{\partial \text{CRLB}(\hat{\theta})}{\partial P_{n,m,\tilde{s}}}\right|$, it can be rewritten as $\lambda_4 < 1 - \left(\frac{\tau_{\max}^2\left|\frac{\partial f(\mathbf{P})}{\partial P_{n,m,\tilde{s}}}\right| - |\lambda_1|}{\tau_{\max}^2\left|\frac{\partial f(\mathbf{P})}{\partial P_{n,m,\tilde{s}}}\right| - \left|\frac{\partial \text{CRLB}(\hat{\theta})}{\partial P_{n,m,\tilde{s}}}\right|}\right) > 0$. Since this needs to be satisfied for all $\{n, m, \tilde{s}\}$ pairs, $\lambda_1$ is chosen as $|\lambda_1| > \left|\frac{\partial \text{CRLB}(\hat{\theta})}{\partial P_{n_{\max}, m_{\max}, \tilde{s}_{\max}}}\right| = \max\left\{\left|\frac{\partial \text{CRLB}(\hat{\theta})}{\partial P_{1,1,1}}\right|, \ldots, \left|\frac{\partial \text{CRLB}(\hat{\theta})}{\partial P_{N,M,U_{\text{rad}}}}\right|\right\}$, and subsequently the corresponding $\lambda_4$ can be calculated so that the KKT condition in (72) is satisfied. All KKT conditions are then satisfied, and the minimum $\text{CRLB}(\hat{\theta})$ is given by (59).

## REFERENCES

[1] T. Wild, V. Braun, and H. Viswanathan, "Joint design of communication and sensing for beyond 5G and 6G systems," *IEEE Access*, vol. 9, pp. 30 845–30 857, Feb. 2021.

[2] C. Baquero Barneto, T. Riihonen, M. Turunen, L. Anttila, M. Fleischer, K. Stadius, J. Ryynänen, and M. Valkama, "Full-duplex OFDM radar with LTE and 5G NR waveforms: Challenges, solutions, and measurements," *IEEE Transactions on Microwave Theory and Techniques*, vol. 67, no. 10, pp. 4042–4054, Oct. 2019.

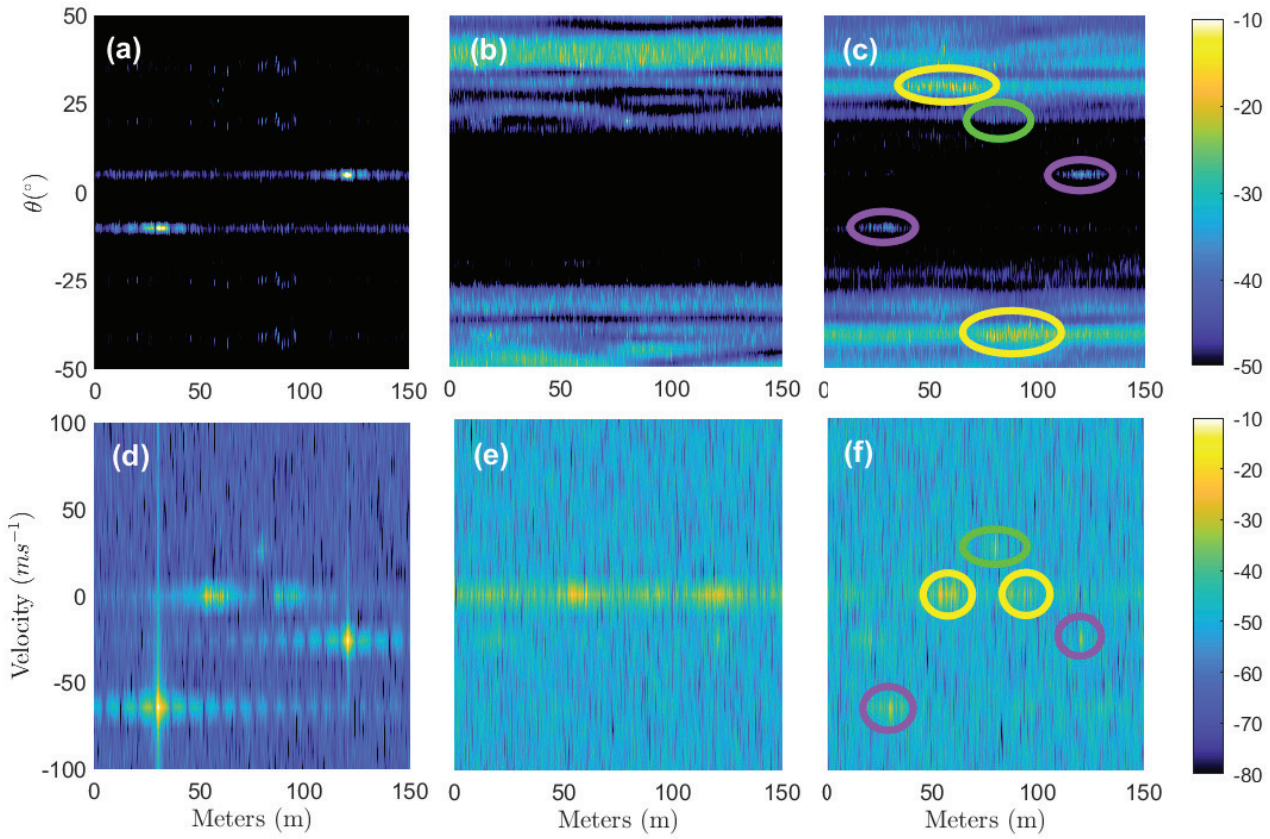


Fig. 7. Range–angle maps for: (a) $\rho, \beta = 0$ (sensing only), (b) $\rho, \beta = 1$ (communications only), and (c) $\rho, \beta = 0.5$ (JCAS), and range–velocity maps for : (d) $\rho, \beta = 0$, (e) $\rho, \beta = 1$, and (f) $\rho, \beta = 0.5$. The colored circles correspond to targets in Fig. 2.

$$\frac{\partial f(\mathbf{P})}{\partial P_{n,m,\tilde{s}}} = \frac{4(\Delta f)^2}{\cos^2(\theta)} \left( \frac{\bar{n}^2 |g_{n,m,\tilde{s}}|^2}{\sum_{m=1}^{M} \sum_{n=1}^{N} \sum_{s=1}^{S} P_{n,m,s} (\mathbf{g}'_{n,m,s})^H \mathbf{g}'_{n,m,s}} - \frac{\sum_{m=1}^{M} \sum_{n=1}^{N} \sum_{s=1}^{S} \bar{n}^2 P_{n,m,s} (\mathbf{g}_{n,m,s})^H \mathbf{g}_{n,m,s} |g'_{n,m,\tilde{s}}|^2}{\left( \sum_{m=1}^{M} \sum_{n=1}^{N} \sum_{s=1}^{S} P_{n,m,s} (\mathbf{g}'_{n,m,s})^H \mathbf{g}'_{n,m,s} \right)^2} \right) \tag{69}$$

$$1 \gtrless \underbrace{\left( \frac{P_{n,m,\tilde{s}} (\mathbf{g}'_{n,m,\tilde{s}})^H \mathbf{g}'_{n,m,\tilde{s}}}{\sum_{m=1}^{M} \sum_{n=1}^{N} \sum_{s=1}^{S} P_{n,m,s} (\mathbf{g}'_{n,m,s})^H \mathbf{g}'_{n,m,s}} \right)}_{\gamma_1} \underbrace{\left( \frac{\sum_{m=1}^{M} \sum_{n=1}^{N} \sum_{s=1}^{S} \bar{n}^2 P_{n,m,s} (\mathbf{g}_{n,m,s})^H \mathbf{g}_{n,m,s}}{\bar{n}^2 P_{n,m,\tilde{s}} (\mathbf{g}_{n,m,\tilde{s}})^H \mathbf{g}_{n,m,\tilde{s}}} \right)}_{\gamma_2} \tag{70}$$


[3] J. Wang, J. Zhang, Y. Zhang, T. Jiang, L. Yu, and G. Liu, "Empirical analysis of sensing channel characteristics and environment effects at 28 Ghz," in *Proc. IEEE Globecom Workshops*, Dec. 2022, pp. 1323–1328.

[4] S. D. Liyanaarachchi, T. Riihonen, C. Baquero Barneto, and M. Valkama, "Optimized waveforms for 5G–6G communication with sensing: Theory, simulations and experiments," *IEEE Transactions on Wireless Communications*, vol. 20, no. 12, pp. 8301–8315, Dec. 2021.

[5] B. Paul, A. R. Chiriyath, and D. W. Bliss, "Survey of RF communications and sensing convergence research," *IEEE Access*, vol. 5, pp. 252–270, Dec. 2016.

[6] C. Baquero Barneto, S. D. Liyanaarachchi, M. Heino, T. Riihonen, and M. Valkama, "Full duplex radio/radar technology: The enabler for advanced joint communication and sensing," *IEEE Wireless Communications*, vol. 28, no. 1, pp. 82–88, Feb. 2021.

[7] S. D. Liyanaarachchi, C. Baquero Barneto, T. Riihonen, and M. Valkama, "Joint OFDM waveform design for communications and sensing convergence," in *Proc. IEEE International Conference on Communications*, Jun. 2020.

[8] J. A. Zhang, M. L. Rahman, K. Wu, X. Huang, Y. J. Guo, S. Chen, and J. Yuan, "Enabling joint communication and radar sensing in mobile networks—A survey," *IEEE Communications Surveys & Tutorials*, vol. 24, no. 1, pp. 306–345, Oct. 2022.

[9] A. R. Chiriyath, B. Paul, and D. W. Bliss, "Radar-communications convergence: Coexistence, cooperation, and co-design," *IEEE Transactions on Cognitive Communications and Networking*, vol. 3, no. 1, Mar. 2017.

[10] M. Bică and V. Koivunen, "Multicarrier radar-communications waveform design for RF convergence and coexistence," in *Proc. IEEE International Conference on Acoustics, Speech and Signal Processing*,

$$\mathcal{L}\left(\mathbf{P},\lambda_1,\boldsymbol{\lambda}_2,\boldsymbol{\lambda}_3,\lambda_4\right)=\mathrm{CRLB}(\hat{\theta})+\lambda_1\left(P_{\mathrm{t}}-P_{\mathrm{com}}-\sum_{m=1}^{M}\sum_{n=1}^{N}\sum_{\tilde{s}=1}^{U_{\mathrm{rad}}}P_{n,m,\tilde{s}}\right)-\sum_{m=1}^{M}\sum_{n=1}^{N}\sum_{\tilde{s}=1}^{U_{\mathrm{rad}}}\lambda_{2,n,m,\tilde{s}}P_{n,m,\tilde{s}}$$
$$+\sum_{m=1}^{M}\sum_{n=1}^{N}\sum_{\tilde{s}=1}^{U_{\mathrm{rad}}}\lambda_{3,n,m,\tilde{s}}(P_{\max}-P_{n,m,\tilde{s}})+\lambda_4\left(\tau_{\max}^2 f(\mathbf{P})-\mathrm{CRLB}(\hat{\theta})\right) \tag{71}$$


May 2019, pp. 7780–7784.

[11] F. Liu, L. Zhou, C. Masouros, A. Li, W. Luo, and A. Petropulu, "Toward dual-functional radar-communication systems: Optimal waveform design," *IEEE Transactions on Signal Processing*, vol. 66, no. 16, pp. 4264–4279, Aug. 2018.

[12] A. Hassanien, M. G. Amin, E. Aboutanios, and B. Himed, "Dual-function radar communication systems: A solution to the spectrum congestion problem," *IEEE Signal Processing Magazine*, vol. 36, no. 5, pp. 115–126, Sep. 2019.

[13] F. Liu, C. Masouros, A. P. Petropulu, H. Griffiths, and L. Hanzo, "Joint radar and communication design: Applications, state-of-the-art, and the road ahead," *IEEE Transactions on Communications*, vol. 68, no. 6, pp. 3834–3862, Jun. 2020.

[14] M. Xiao *et al.*, "Millimeter wave communications for future mobile networks," *IEEE Journal on Selected Areas in Communications*, vol. 35, no. 9, pp. 1909–1935, Sep. 2017.

[15] S. A. Busari, K. M. S. Huq, S. Mumtaz, L. Dai, and J. Rodriguez, "Millimeter-wave massive MIMO communication for future wireless systems: A survey," *IEEE Communications Surveys and Tutorials*, vol. 20, no. 2, pp. 836–869, Dec. 2017.

[16] S. Sun, T. S. Rappaport, R. W. Heath, A. Nix, and S. Rangan, "MIMO for millimeter-wave wireless communications: beamforming, spatial multiplexing, or both?" *IEEE Communications Magazine*, vol. 52, no. 12, pp. 110–121, Dec. 2014.

[17] J. Zhang, E. Björnson, M. Matthaiou, D. W. K. Ng, H. Yang, and D. J. Love, "Prospective multiple antenna technologies for beyond 5G," *IEEE Journal on Selected Areas in Communications*, vol. 38, no. 8, pp. 1637–1660, Aug. 2020.

[18] O. E. Ayach, S. Rajagopal, S. Abu-Surra, Z. Pi, and R. W. Heath, "Spatially sparse precoding in millimeter wave MIMO systems," *IEEE Transactions on Wireless Communications*, vol. 13, no. 3, pp. 1499–1513, Mar. 2014.

[19] Q. Spencer *et al.*, "Zero-forcing methods for downlink spatial multiplexing in multiuser MIMO channels," *IEEE Transactions on Signal Processing*, vol. 52, no. 2, pp. 461–471, Feb. 2004.

[20] S. D. Liyanaarachchi, C. Baquero Barneto, T. Riihonen, M. Heino, and M. Valkama, "Joint multi-user communication and MIMO radar through full-duplex hybrid beamforming," in *Proc. IEEE International Online Symposium on Joint Communications & Sensing*, Feb. 2021.

[21] W. Ni and X. Dong, "Hybrid block diagonalization for massive multiuser MIMO systems," *IEEE Transactions on Communications*, vol. 64, no. 1, pp. 201–211, Jan. 2016.

[22] A. M. Haimovich, R. S. Blum, and L. J. Cimini, "MIMO radar with widely separated antennas," *IEEE Signal Processing Magazine*, vol. 25, no. 1, pp. 116–129, Dec. 2007.

[23] J. Li and P. Stoica, "MIMO radar with colocated antennas," *IEEE Signal Processing Magazine*, vol. 24, no. 5, pp. 106–114, Sep. 2007.

[24] K. Forsythe, D. Bliss, and G. Fawcett, "Multiple-input multiple-output (MIMO) radar: performance issues," in *Proc. Asilomar Conference on Signals, Systems and Computers*, Nov. 2004, pp. 310–315.

[25] D. Bliss and K. Forsythe, "Multiple-input multiple-output (MIMO) radar and imaging: degrees of freedom and resolution," in *Proc. Asilomar Conference on Signals, Systems & Computers*, Nov. 2003, pp. 54–59.

[26] S. Xu, J. Wang, and A. Yarovoy, "Super resolution DOA for FMCW automotive radar imaging," in *Proc. IEEE Conference on Antenna Measurements Applications*, Sep. 2018.

[27] F. Liu, C. Masouros, A. Li, H. Sun, and L. Hanzo, "MU-MIMO communications with MIMO radar: From co-existence to joint transmission," *IEEE Transactions on Wireless Communications*, vol. 17, no. 4, pp. 2755–2770, Apr. 2018.

[28] M. Bică and V. Koivunen, "Radar waveform optimization for target parameter estimation in cooperative radar-communications systems," *IEEE Transactions on Aerospace and Electronic Systems*, vol. 55, no. 5, pp. 2314–2326, Oct. 2019.

[29] A. Ahmed, Y. D. Zhang, A. Hassanien, and B. Himed, "OFDM-based joint radar-communication system: Optimal sub-carrier allocation and power distribution by exploiting mutual information," in *Proc. Asilomar Conference on Signals, Systems, and Computers*, Nov. 2019, pp. 559–563.

[30] C. Sturm, T. Zwick, and W. Wiesbeck, "An OFDM system concept for joint radar and communications operations," in *Proc. IEEE 69th Vehicular Technology Conference*, Apr. 2009, pp. 1–5.

[31] S. Buzzi, C. D'Andrea, and M. Lops, "Using massive MIMO arrays for joint communication and sensing," in *Proc. Asilomar Conference on Signals, Systems, and Computers*, Nov. 2019, pp. 5–9.

[32] M. F. Keskin, H. Wymeersch, and V. Koivunen, "MIMO-OFDM joint radar-communications: Is ICI friend or foe?" *IEEE Journal of Selected Topics in Signal Processing*, vol. 15, no. 6, pp. 1393–1408, Nov. 2021.

[33] F. Wang and H. Li, "Power allocation for coexisting multicarrier radar and communication systems in cluttered environments," *IEEE Transactions on Signal Processing*, vol. 69, pp. 1603–1613, Feb. 2021.

[34] X. Gao, L. Dai, S. Han, C. I, and R. W. Heath, "Energy-efficient hybrid analog and digital precoding for mmwave MIMO systems with large antenna arrays," *IEEE Journal on Selected Areas in Communications*, vol. 34, no. 4, pp. 998–1009, Apr. 2016.

[35] F. Liu and C. Masouros, "Hybrid beamforming with sub-arrayed MIMO radar: Enabling joint sensing and communication at mmwave band," in *Proc. IEEE International Conference on Acoustics, Speech and Signal Processing*, May 2019, pp. 7770–7774.

[36] A. Kaushik, C. Masouros, and F. Liu, "Hardware efficient joint radar-communications with hybrid precoding and RF chain optimization," in *Proc. IEEE International Conference on Communications*, Jun. 2021.

[37] X. Wang, Z. Fei, J. A. Zhang, and J. Xu, "Partially-connected hybrid beamforming design for integrated sensing and communication systems," *IEEE Transactions on Communications*, vol. 70, no. 10, pp. 6648–6660, Oct. 2022.

[38] S. D. Liyanaarachchi, C. Baquero Barneto, T. Riihonen, M. Heino, and M. Valkama, "Range–angle processing for target detection in joint MIMO-OFDM communications and sensing," in *Proc. IEEE International Workshop on Signal Processing Advances in Wireless Communications*, Sep. 2021, pp. 486–490.

[39] "3GPP TS 38.104 v17.5.0, "NR; Base Station (BS) radio transmission and reception", Tech. Spec. Group Radio Access Network, Rel. 17," Mar. 2022.

[40] R. W. Heath, N. González-Prelcic, S. Rangan, W. Roh, and A. M. Sayeed, "An overview of signal processing techniques for millimeter wave MIMO systems," *IEEE Journal of Selected Topics in Signal Processing*, vol. 10, no. 3, pp. 436–453, Feb. 2016.

[41] M. Wax and T. Kailath, "Detection of signals by information theoretic criteria," *IEEE Transactions on Acoustics, Speech, and Signal Processing*, vol. 33, no. 2, pp. 387–392, Apr. 1985.

[42] H.-T. Wu, J.-F. Yang, and F.-K. Chen, "Source number estimators using transformed Gerschgorin radii," *IEEE Transactions on Signal Processing*, vol. 43, no. 6, pp. 1325–1333, Jun. 1995.

[43] S. M. Kay, *Fundamentals of Statistical Signal Processing: Detection Theory*. Prentice Hall, 1998.

[44] ——, *Fundamentals of Statistical Signal Processing: Estimation Theory*. Prentice Hall, 1993.

[45] J. A. Zhang, X. Huang, Y. J. Guo, J. Yuan, and R. W. Heath, "Multibeam for joint communication and radar sensing using steerable analog antenna arrays," *IEEE Transactions on Vehicular Technology*, vol. 68, no. 1, pp. 671–685, Jan. 2019.

[46] W. Ni and X. Dong, "Hybrid block diagonalization for massive multiuser MIMO systems," *IEEE Transactions on Communications*, vol. 64, no. 1, pp. 201–211, Jan. 2016.

## BIOGRAPHIES

**Sahan Damith Liyanaarachchi** [S'16] is a Radio Research Scientist at the Nokia Bell Labs, Espoo, Finland. He will receive his D.Sc. degree in communications engineering in late summer 2023 from the Tampere University, Finland. He received his B.Sc. and M.Sc. degrees (both with honors) from University of Peradeniya, Sri Lanka, and Tampere University, Finland, in 2016 and 2019, respectively. His research interests include radio communications, radio localization, and radio-based sensing with current interest in the evolution of 6G technology.

**Taneli Riihonen** [S'06, M'14, SM'22] received his D.Sc. degree in electrical engineering (with honors) from Aalto University, Helsinki, Finland, in 2014. He is currently a tenure-track Associate Professor at the Faculty of Information Technology and Communication Sciences, Tampere University, Finland. His research activity is focused on physical-layer analysis, link-layer techniques and signal processing for all kinds of radio systems from consumer and commercial domains to defense and security with current interest in the evolution of 6G technology.

**Carlos Baquero Barneto** [S'18] received the B.Sc. and M.Sc. degrees in telecommunication engineering from Universidad Politécnica de Madrid, Spain, in 2017 and 2018, respectively, and the D.Sc. degree from Tampere University, Finland. His research interests include joint communication and sensing systems' design, with particular emphasis on 5G and beyond mobile radio networks.

**Mikko Valkama** [S'00, M'01, SM'15, F'22] received his M.Sc. (Tech.) and D.Sc. (Tech.) degrees (both with honors) from Tampere University of Technology, Finland, in 2000 and 2001, respectively. Currently, he is a Full Professor and the Head of the Unit of Electrical Engineering at the newly formed Tampere University, Finland. His general research interests include radio communications, radio localization, and radio-based sensing, with particular emphasis on 5G and 6G mobile radio networks.